Sterically Stabilized End-On Superoxocopper(II) Complexes and Mechanistic Insights Into Their Reactivity With O-H, N-H and C-H Substrates.

Sebastian Y. Quek,[a],‡ Suman Debnath,[a],‡ Shoba Laxmi,[a],‡ Maurice van Gastel,[b] and Jason England.[a],*

[a] Division of Chemistry and Biological, School of Physical and Mathematical Sciences, Nanyang Technological University, 21 Nanyang Link, Singapore 637371.

[b] Max-Planck-Institut für Kohlenforschung, Kaiser-Wilhelm-Platz, Mülheim an der Ruhr, D-45470, Germany.

ABSTRACT: Instability of end-on superoxocopper(II) complexes, with respect to conversion to the corresponding peroxo-bridged complexes, has largely constrained their study to very low temperatures (< -80°C). This limits their kinetic capacity to oxidize substrates. In response, we have developed a series of ligand systems bearing bulky aryl substituents that are primarily directed away from the metal centre, Ar_3-TMPA (Ar = tpb, dpb, dtbpb), and used them to support $[Cu^{I}(Ar_3\text{-TMPA})(NCMe)]^+$ copper(I) complexes. Solutions of all three react with O_2 to yield $[Cu^{II}(\eta^1\text{-}O_2^{\bullet-})(Ar_3\text{-TMPA})]^+$ complexes that are stable against dimerization at all temperatures. Full binding of O_2 is observed at sub-ambient temperatures and can be reversed by warming. The onset of oxygenation is ligand dependent, but can be observed at 25°C in the case of Ar = tpb and dpb. Furthermore, all three $[Cu^{II}(\eta^1\text{-}O_2^{\bullet-})(Ar_3\text{-TMPA})]^+$ complexes are stable against self-decay at temperatures ≤ -20°C. This provides a wide temperature window over which these complexes can be studied, which was exploited by performing extensive reaction kinetics measurements for $[Cu^{II}(\eta^1\text{-}O_2^{\bullet-})(tpb_3\text{-TMPA})]^+$ with a broad range of O-H, N-H, and C-H bond substrates. This includes correlation of second order rate constants (k_2 values) versus oxidation potentials (E_{ox}) for a range of phenols (i.e., a Marcus plot), construction of Eyring plots, and temperature-dependent kinetic isotope effect (KIE) measurements. The data obtained indicates that reaction with all substrates proceeds via H-atom transfer (HAT) to $[Cu^{II}(\eta^1\text{-}O_2^{\bullet-})(tpb_3\text{-TMPA})]^+$. In addition, evidence suggests that HAT reaction with the phenols studied proceeds with significant charge transfer, and that it involves full tunelling of both H and D atoms in the case of 1,2-diphenylhydrazine (DPH) and 4-methoxy-2,6-di-tert-butylphenol (MeO-ArOH). Consistent with expectations for HAT, large entropic barriers ($\Delta S^{\ddagger}$) were measured for the substrates MeO-ArOH, DPH, triphenylhydrazine (TPH), and 1-benzyl-1,4-dihydronicotinamide (BNAH). Despite having the lowest X-H bond dissociation energy (BDE) amongst these substrates, the C-H substrate BNAH exhibits both the largest $\Delta S^{\ddagger}$ and the second largest enthalpic barrier ($\Delta H^{\ddagger}$) to reaction. This is congruent with the expectation that oxidation of C-H bonds is kinetically challenging and the experimental observation that $[Cu^{II}(\eta^1\text{-}O_2^{\bullet-})(tpb_3\text{-TMPA})]^+$ is only able to oxidize very weak C-H bonds, whereas it can oxidize moderately strong N-H bonds.

INTRODUCTION

End-on superoxocopper(II) species, $Cu^{II}(\eta^1\text{-}O_2^{\bullet-})$, have been forwarded as intermediates in a wide range of O_2 activating copper-containing enzymes.[1-2] This includes the monometallic enzyme galactose oxidase (GO), wherein a $Cu^{II}(\eta^1\text{-}O_2^{\bullet-})$ species is accepted to be responsible for hydrogen atom abstraction (HAA) from a tyrosine residue to yield a catalytically crucial copper-coordinated phenoxyl radical.[3-5] There are also a number of oxygenases in which $Cu^{II}(\eta^1\text{-}O_2^{\bullet-})$ intermediates are evidenced to be responsible for initial HAA from substrate C-H bonds of moderate strength. More specifically, the non-coupled binuclear copper enzymes peptidylglycine α-hydroxylating monooxygenase (PHM), dopamine β-monooxygenase (DβM), and tyramine β-monooxygenase (TβM), which are responsible for hydroxylation of activated methylene units;[1, 6-7] and the monocopper formylglycine-generating enzyme (FGE), which catalytically converts cysteine to formylglycine at an active site possessing an unusual dicysteinate-coordinated copper(I) resting state.[8-9] Of these systems, PHM and DβM are the most comprehensively studied, with some of the highlights being kinetic isotope effect (KIE) studies confirming that C-H oxidation occurs prior to O-O bond cleavage,[10-12] measurement of "intrinsic" substrate KIEs of 10 – 12,[11, 13-14] evidence that hydrogen atom transfer (HAT) proceeds via quantum tunneling,[15] and an X-ray structure of PHM showing end-on coordination of O_2 to the substrate binding site Cu_M.[16] Strong support for the proposed mode of operation of the non-coupled binuclear copper enzymes, including the intermediacy of $Cu^{II}(\eta^1\text{-}O_2^{\bullet-})$ active oxidants, has been provided by DFT calculations.[17-18]

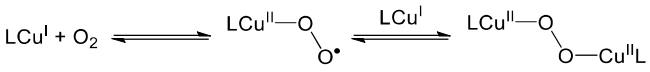

Scheme 1. Copper-O_2 reactivity relevant to this study.

The importance of $Cu^{II}(\eta^1\text{-}O_2^{\bullet-})$ intermediates in enzymatic systems and their potential synthetic utility has

spurred significant efforts to synthesize and study the reactivity of 1:1 adducts of Cu and O_2. Although significant numbers of $Cu^{II}(\eta^1\text{-}O_2^{\bullet-})$ model complexes have now been reported (see refs [19-20] for comprehensive reviews of the field), exploration of their reactivity properties is not without difficulties. This is, in large part, due to their tendency to collapse to thermodynamically favored species of higher nuclearity, such as peroxo-bridged dicopper(II) complexes, $Cu^{II}(\mu^2\text{-}O_2^{2-})Cu^{II}$ (Scheme 1). To retard the aforementioned "dimerization" reaction and avoid other decay processes, such as ligand oxidation, study of $Cu^{II}(\eta^1\text{-}O_2^{\bullet-})$ complexes is overwhelmingly conducted at very low temperatures (< -80°C). For example, in seminal work by Karlin and Zuberbühler it was shown that reaction of $[Cu^{I}(TMPA)(NCMe)]^+$ (Chart 1) with O_2 at temperatures between -75 and -90°C rapidly forms the corresponding $Cu^{II}(\mu^2\text{-}O_2^{2-})Cu^{II}$ complex.[21-22] The $[Cu^{II}(\eta^1\text{-}O_2^{\bullet-})(TMPA)]^+$ species was observed as a transient intermediate, using stopped-flow kinetics, but low temperatures of -135°C were required to accumulate significant amounts of it.[23] Even then, it was obtained as a mixture with, and slowly converts to, the corresponding $Cu^{II}(\mu^2\text{-}O_2^{2-})Cu^{II}$ complex.

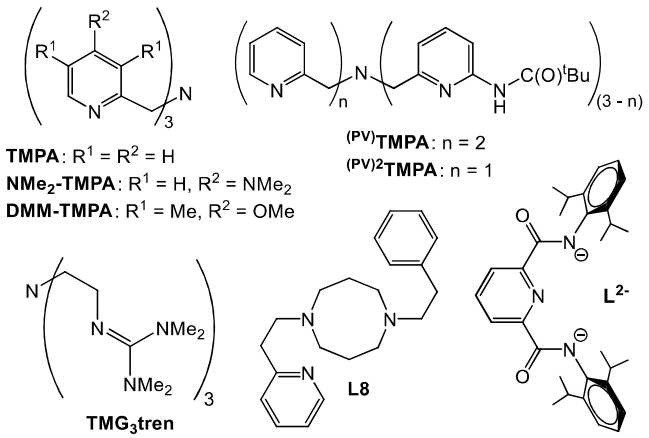

Chart 1. Selected ligands that have been used to support $Cu^{II}(\eta^1\text{-}O_2^{\bullet-})$ complexes.

The simplest method of prohibiting formation of 2:1 adducts of Cu and O_2 (and higher nuclearity species) is to employ sterically encumbered ligands. This has proven particularly successful for monoanionic bidentate and tridentate ligand architectures, which tend to favor formation of side-on bound (η^2) 1:1 adducts of Cu and O_2. These $Cu(\eta^2\text{-}O_2)$ species are (in general) much more stable than their $Cu^{II}(\eta^1\text{-}O_2^{\bullet-})$ analogues and, concordantly, several $Cu^{II}(\eta^2\text{-}O_2^{\bullet-})$ or $Cu^{III}(\eta^2\text{-}O_2^{2-})$ complexes have been isolated and crystallographically characterized.[24-30] Unfortunately, this comparatively high stability equates to low intermolecular reactivity. Indeed, the only exception, Beltey's dipyrrin-supported $Cu^{II}(\eta^2\text{-}O_2^{\bullet-})$ complex, is believed to react with substrates via a thermally driven isomerization to the corresponding $Cu^{II}(\eta^1\text{-}O_2^{\bullet-})$ species.[27]

Sterically encumbered ligands are also effective at stabilizing $Cu^{II}(\eta^1\text{-}O_2^{\bullet-})$ moieties, with the most graphic demonstration being Schindler and coworkers' synthesis of $[Cu^{II}(\eta^1\text{-}O_2^{\bullet-})(TMG_3tren)]^+$ (Chart 1).[31] Not only was this complex fully stable against formation of higher nuclearity species, but it was formed via a fully reversible oxygenation reaction, and the superoxocopper(II) complex was sufficiently stable for crystallographic characterization.[32-33] Unfortunately, like most other sterically stabilized systems,[34-35] it was found to display limited HAA reactivity with substrates.[36] This may not be due to steric factors alone, with the high basicity of the guanidine donors likely to impact reactivity significantly. Consistent with this notion, Tolman's complex $[Cu^{II}(\eta^1\text{-}O_2^{\bullet-})(L)]^-$, supported by a dianionic 2,6-dicarboxamidopyridine ligand (Chart 1),[35] performs HAA only from weak O-H bonds. In other circumstances, it tends to favor nucleophilic reaction (primarily protonation).[37-39]

To date, the most diverse array of reactivity displayed by a single system was reported for Itoh's complex $[Cu^{II}(\eta^1\text{-}O_2^{\bullet-})(L8)]^+$ (Chart 1).[40] It oxidizes a range of electron transfer agents, which allowed estimation of its reduction potential, it performs oxo-atom transfer to phosphines, and it reacts with phenols via protonolysis and TEMPO-H to yield the corresponding hydroperoxocopper(II) complex.[41] In addition, $[Cu^{II}(\eta^1\text{-}O_2^{\bullet-})(L8)]^+$ undergoes self-decay via intramolecular hydroxylation of the benzylic position of its pendant ethylbenzene substitutent, for which a KIE and Eyring parameters were measured.[42-43] The unique reactivity of this system has been attributed to the close resemblance of its *pseudo*-tetrahedral coordination geometry to that of the O_2 activating Cu_M site of the non-coupled binuclear copper monooxygenases.[40]

However, the most extensive substrate reactivity studies reported for $Cu^{II}(\eta^1\text{-}O_2^{\bullet-})$ model complexes are those of Karlin and co-workers, which revolve around derivatives of the TMPA ligand system (Chart 1). They demonstrated that introduction of electron donating[44-46] and hydrogen bond donor[23, 47] functionality into this ligand framework can "stabilize" the $Cu^{II}(\eta^1\text{-}O_2^{\bullet-})$ moiety, by slowing or eliminating conversion to $Cu^{II}(\mu^2\text{-}O_2^{2-})Cu^{II}$ complexes. This provided a means to study reaction of the corresponding $Cu^{II}(\eta^1\text{-}O_2^{\bullet-})$ complexes with a wide array of substrates. For instance, extensive mechanistic studies for reaction of $[Cu^{II}(\eta^1\text{-}O_2^{\bullet-})(DMM\text{-}TMPA)]^+$ with phenolic substrates were

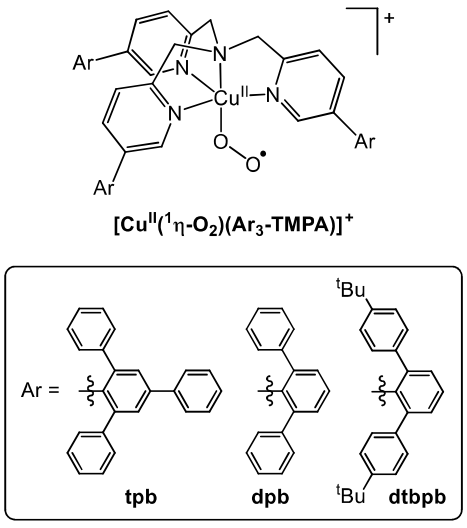

Figure 1. The $Cu^{II}(\eta^1\text{-}O_2^{\bullet-})$ complexes studied herein.

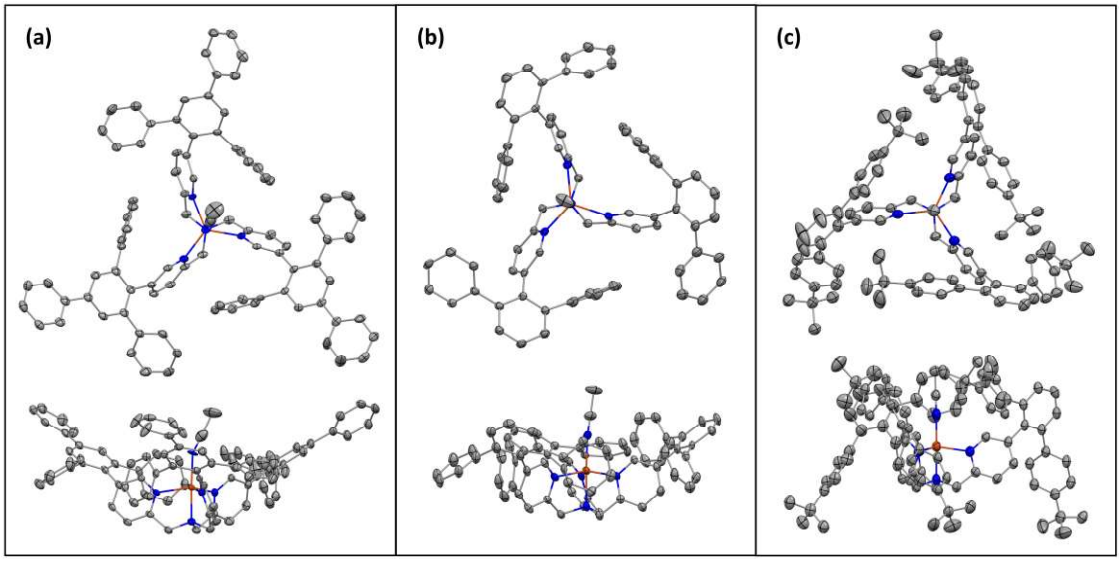

Figure 2. Top and side views (above and below, respectively) of X-ray crystal structures of **(a)** [Cu^{II}(tpb$_3$-TMPA)(NCMe)](ClO_4)$_2$, **(b)** [Cu^{II}(dpb$_3$-TMPA)(NCMe)](ClO_4)$_2$ and **(c)** [Cu^{II}(dtbpb$_3$-TMPA)(NCMe)](OTf)$_2$, depicted using 50 % thermal ellipsoids. Hydrogen atoms, counteranions and solvent molecules have been omitted for clarity. Gray, blue and orange spheroids correspond to carbon, nitrogen, and copper atoms, respectively.

conducted.[46] This included measurement of rate constants over a 15°C temperature range, from -85 to -100°C, which allowed construction of an Eyring plot. More recently, introduction of H-bond donor substituents at the 6-position of the pyridine donors was shown to significantly enhance reactivity. A single pivaloyl functional group, giving $^{(PV)}$TMPA (Chart 1), allows HAA from the weak C-H bonds of 1-benzyl-1,4-dihydronicotinamide (BNAH) and 1,3-dimethyl-2,3-dihydrobenzimidazole (BzImH), and the comparatively strong O-H bond of 4-methoxyphenol.[23, 47] Furthermore, the inclusion of two pivaloyl groups, giving $^{(PV)2}$TMPA (Chart 1), allows reaction with the stronger C-H bonds of dihydroanthracene and fluorene at -135°C.[48]

With the aforementioned factors in mind, we sought to stabilize a TMPA-supported $Cu^{II}(\eta^1\text{-}O_2^{\bullet-})$ complex via introduction of bulky substituents, but in such a way that steric inhibition of reaction with substrates is minimized. To this end, we installed a series of bulky aryl substituents onto the 5-position of the pyridine rings to give the Ar$_3$-TMPA ligands (Figure 1). The formation and stability of the resulting [$Cu^{II}(\eta^1\text{-}O_2^{\bullet-})$(tpb$_3$-TMPA)]$^+$ complexes, where Ar = 2,4,6-triphenylbenzene (tpb), 2,6-diphenylbenzene (dpb), and 2,6-di(4-tert-butylphenyl)benzene (dtbpb), plus their reactivity with a broad range of O-H, N-H, and C-H bond substrates, are detailed herein.

RESULTS AND DISCUSSION

In addition to the [Cu^{I}(Ar$_3$-TMPA)(NCMe)][$B(C_6F_5)_4$] (Ar = tpb, dpb, and dtbpb) copper(I) complexes employed in the oxygenation studies described below, copper(II) complexes of formulation [Cu^{II}(Ar$_3$-TMPA)(NCMe)](Y)$_2$ (Y^- = ClO_4^- or TfO^-) were prepared. Attempts to grow crystals suitable for X-ray crystallography were only successful for the latter series. As expected, the dicationic components of [Cu^{II}(tpb$_3$-TMPA)(NCMe)](ClO_4)$_2$, [Cu^{II}(dpb$_3$-TMPA)(NCMe)](ClO_4)$_2$, and [Cu^{II}(dtbpb$_3$-TMPA)(NCMe)](OTf)$_2$ all display trigonal bipyramidal geometries (τ_5[49] = 0.97, 0.80, and 1.00, respectively), with the TMPA ligands coordinating in a tripodal tetradentate fashion and the remaining axial coordination site filled by an acetonitrile ligand (Figures 2 and S16 – S18). Crystallographic data and selected structural parameters are listed in the Supporting Information, in Tables S1 – S4.

It is clear from the X-ray structures that the bulky Ar substituents groups primarily point away from the metal centre, and only in the case of dtbpb$_3$-TMPA do they crowd the MeCN-occupied axial coordination site to a readily appreciable extent. Instead of projecting vertically, parallel to the Cu–NCMe axis, the steric bulk is predominantly oriented laterally, perpendicular to the Cu–NCMe axis. It was anticipated that this would provide inter-donor repulsion, whilst minimizing the decrease in donor strength that usually accompanies introduction of steric bulk.

Although the respective average Cu–$N_{pyridine}$ bond lengths in [Cu^{II}(tpb$_3$-TMPA)(NCMe)]$^{2+}$, [Cu^{II}(dpb$_3$-TMPA)(NCMe)]$^{2+}$ and [Cu^{II}(dtbpb$_3$-TMPA)(NCMe)]$^{2+}$ of 2.067(3), 2.071(5), and 2.060(4) Å may be marginally longer than the corresponding distance of 2.042(4) Å in the parent compound [Cu^{II}(TMPA)(NCMe)]$^{2+}$,[50] the values are sufficiently similar to argue that the impact of the aryl substituents is minimal. In contrast, introduction of phenyl rings onto the 6-position of the pyridine donors in the parent TMPA ligand causes elongation of the average Cu–$N_{pyridine}$ distance in the corresponding copper(II) complex, [Cu^{II}(6-Ph$_3$-TMPA)(NCMe)]$^{2+}$, to 2.108(7) Å.[51] This represents an obvious weakening of pyridine-to-Cu donation.

Cyclic voltammetry measurements (Figure S19, Table 1) are consistent with the assertion that the aryl substituents in the [Cu^{II}(Ar$_3$-TMPA)(NCMe)]$^{2+}$ complexes do not significantly weaken with the donor ability of the pyridine rings. More specifically, the half-wave potentials ($E_{1/2}$)

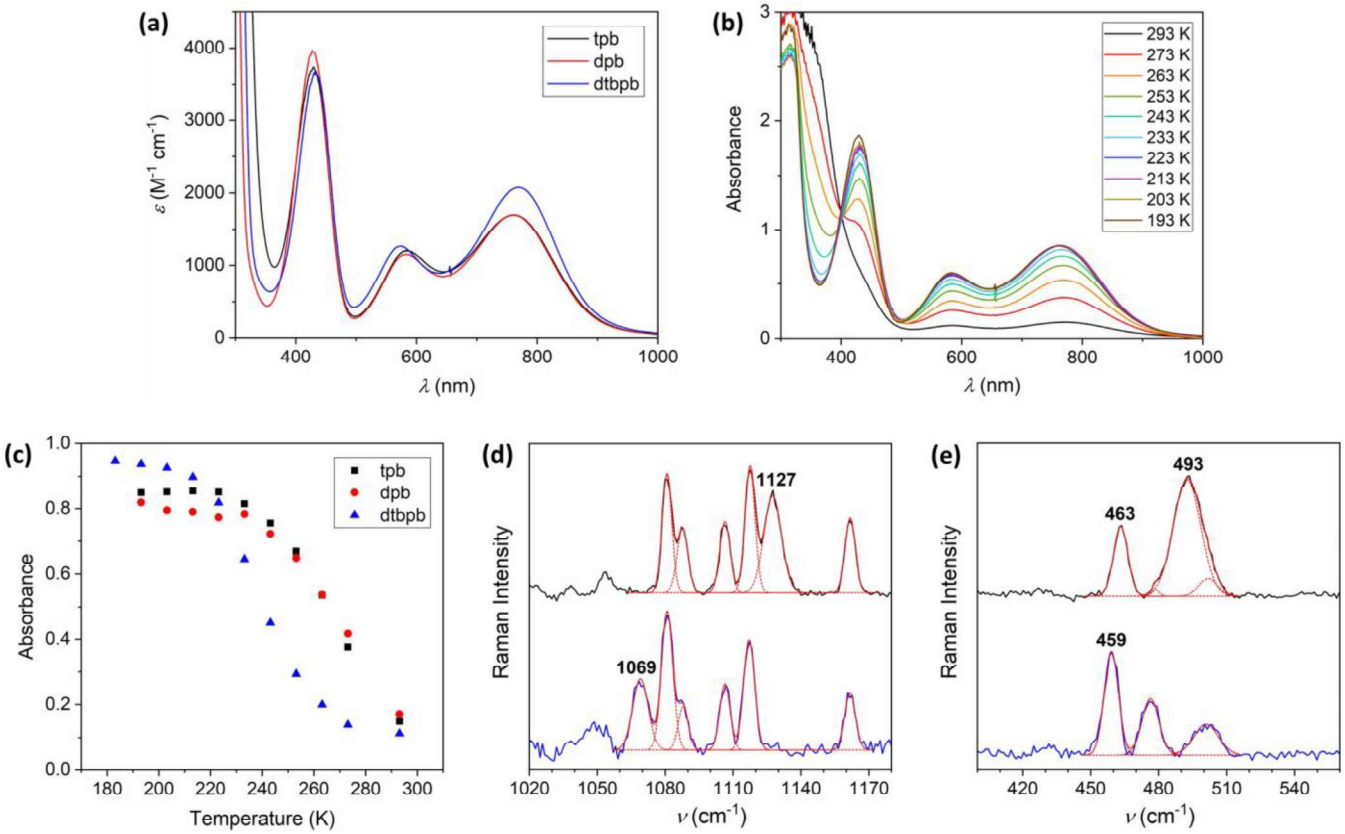

Figure 3. (a) UV-Vis spectra of $[Cu^{II}(\eta^1\text{-}O_2^{\bullet-})(Ar_3\text{-}TMPA)]^+$ (Ar = tpb, dpb, and dtbpb), recorded in THF solution at -80°C. **(b)** UV-vis spectra of O_2 saturated THF solutions of $[Cu^{I}(tpb_3\text{-}TMPA)(NCMe)]^+$ (*ca.* 0.5 mM) and **(c)** absorbances at the 760 – 771 nm λ_{max} of all three $[Cu^{II}(\eta^1\text{-}O_2^{\bullet-})(Ar_3\text{-}TMPA)]^+$ (Ar = tpb, dpb, and dtbpb) complexes, measured at 20°C and regular intervals over the temperature range of 0 to -90°C. Expansions of the **(d)** ν(O-O) and **(e)** ν(Cu-O) containing regions of the resonance Raman spectra (λ_{ex} = 405 nm) of frozen d_8-THF solutions of $[Cu^{II}(\eta^1\text{-}^{16}O_2^{\bullet-})(tpb_3\text{-}TMPA)]^+$ (black lines) and $[Cu^{II}(\eta^1\text{-}^{18}O_2^{\bullet-})(tpb_3\text{-}TMPA)]^+$ (blue lines). Solid and dashed red lines correspond to spectral simulations and Gaussians that comprise the simulations, respectively.

Table 1. Half-wave potentials ($E_{1/2}$) of the Cu^{II}/Cu^{I} redox couples of $[Cu^{II}(Ar_3\text{-}TMPA)(NCMe)]^{2+}$ (Ar = tpb, dpb and dtbpb) and selected complexes.[a]

$[Cu^{II}(L)(NCMe)]^{2+}$, L =	$E_{1/2}$ (V, vs Fc^+/Fc^0)	Ref.
tpb_3-TMPA	-0.39	This work
dpb_3-TMPA	-0.41	This work
$dtbpb_3$-TMPA	-0.32	This work
TMPA	-0.40	44, 51
6-Ph_3-TMPA	-0.10	51

[a]All data recorded at 298 K, in MeCN solution using 0.1 M NBu_4PF_6 as an electrolyte. $E_{1/2} = (E_{pc} + E_{pa})/2$.

of the Cu^{II}/Cu^{I} redox couples of the Ar = tpb and dpb complexes (-0.39 and -0.41 V vs Fc^+/Fc^0) are essentially identical to the value of -0.40 V reported for $[Cu^{II}(TMPA)(NCMe)]^{2+}$.[44, 51] The $E_{1/2}$ of -0.32 V measured for the Ar = dtbpb is more positive than the aforementioned values and indicates destabilization of the Cu^{II} oxidation state, but this cathodic shift is small compared to systems possessing substituents on the 6-position of the pyridine donors. For example, the corresponding $E_{1/2}$ value for $[Cu^{II}(6\text{-}Ph_3\text{-}TMPA)(NCMe)]^{2+}$ is -0.10 V.[51]

Superoxocopper(II) complex formation. It was found that pale yellow solutions of all three $[Cu^{I}(Ar_3\text{-}TMPA)(NCMe)][B(C_6F_5)_4]$ copper(I) complexes react rapidly with O_2 at -80°C in a broad range of organic solvents, including THF, MeTHF, acetone, toluene and diethyl ether, to yield green species. Full oxygenation took less than 10 seconds in THF. The UV-Vis spectra of the three green species closely resemble one another, with three prominent bands centred at approximately (λ_{max}) 430, 580 and 760 nm (Figure 3a and Table 2). These features are diagnostic of end-on superoxocopper(II) complex formation, and are very similar to those of the parent complex $[Cu^{II}(\eta^1\text{-}O_2^{\bullet-})(TMPA)]^+$ (λ_{max} = 410 and 747 nm, with respective ε_{max} = 4000 and 1000 M^{-1} cm^{-1}).[21]

Confirmation of assignment of these green species as $[Cu^{II}(\eta^1\text{-}O_2^{\bullet-})(Ar_3\text{-}TMPA)]^+$ complexes was provided by resonance Raman measurements (Figures 3d and 3e, and Figures S23 – S28). With laser excitation at a wavelength (λ_{ex}) of 405 nm, vibrational bands were observed at 1127 – 1119 cm^{-1} and found to shift to 1069 – 1059 cm^{-1} upon use of $^{18}O_2$ (Table 2). This is very similar to the O-O stretching frequencies, ν(O-O), reported for other $Cu^{II}(\eta^1\text{-}O_2^{\bullet-})$

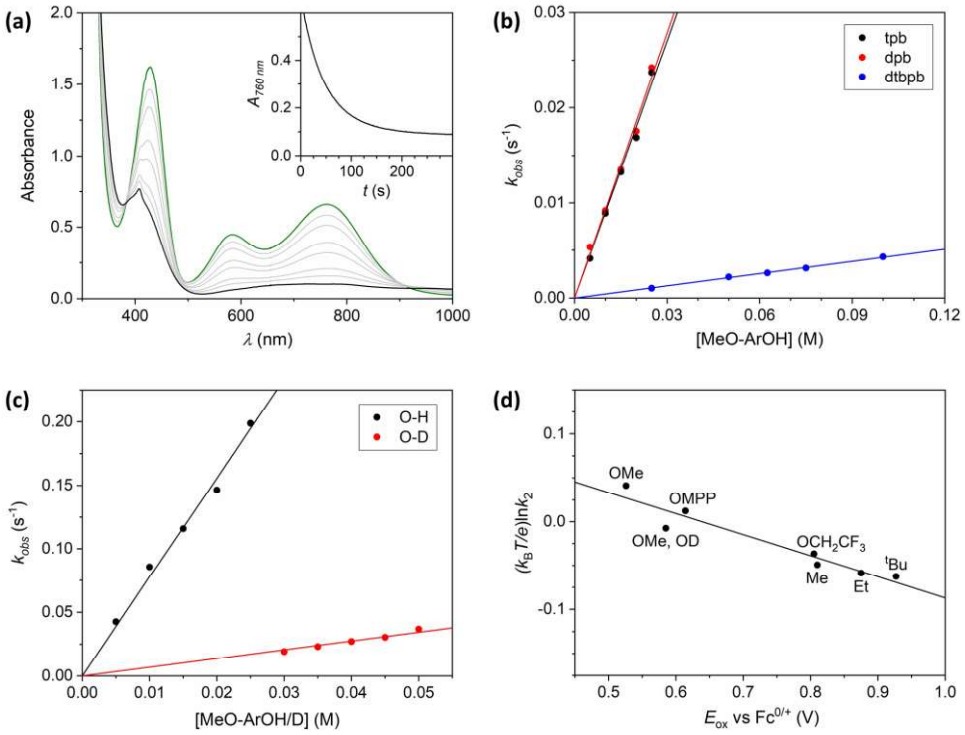

Figure 4. (a) Reaction of $[Cu^{II}(\eta^1\text{-}O_2^{\bullet-})(tpb_3\text{-}TMPA)]^+$ with 4-methoxy-2,6-di-tert-butylphenol (MeO-ArOH), in THF solution at -70°C. Main: UV-Vis spectra of the starting complex, product, and those recorded during the course of reaction are depicted using green, black, and grey lines, respectively. Inset: Absorbance at 760 nm as a function of time. **(b)** Plot of observed rate constants (k_{obs}, s^{-1}) versus substrate concentration (M) for reaction of $[Cu^{II}(\eta^1\text{-}O_2^{\bullet-})(Ar_3\text{-}TMPA)]^+$ (Ar = tpb, dpb, and dtbpb) with MeO-ArOH, in THF solution at -70°C. **(c)** Plot of k_{obs} (s^{-1}) versus substrate concentration (M) for reaction of $[Cu^{II}(\eta^1\text{-}O_2^{\bullet-})(tpb_3\text{-}TMPA)]^+$ with MeO-ArOH and MeO-ArOD (black and red circles, respectively), in THF solution at -40°C. **(d)** Plot of $(k_BT/e)\ln(k_2)$, obtained from reaction of $[Cu^{II}(\eta^1\text{-}O_2^{\bullet-})(tpb_3\text{-}TMPA)]^+$ with 4-substituted 2,6-di-tert-butylphenols (X-ArOH) at -40°C, versus oxidation potentials (E_{ox}, V *vs* Fc^+/Fc^0) of the phenol substrates.

Table 2. A summary of the UV-Vis and resonance Raman spectral features of $[Cu^{II}(\eta^1\text{-}O_2^{\bullet-})(Ar_3\text{-}TMPA)]^+$ (Ar = tpb, dpb, and dtbpb), plus second order rate constants (k_2, $M^{-1}\ s^{-1}$) for reaction of these complexes with 4-methoxy-2,6-di-tert-butylphenol (MeO-ArOH), at -70°C.

Ar	λ_{max}, nm (ε_{max}, $M^{-1}\ cm^{-1}$)[a]	ν(O-O)[b] (cm^{-1})	ν(Cu-O)[b] (cm^{-1})	k_2 ($M^{-1}\ s^{-1}$)
tpb	429 (3740)	1127	482	0.90(5)
	583 (1200)	{-58}	{-23}	
	760 (1700)			
dpb	430(3950)	1126	467	0.93(5)
	584 (1150)	{-63}	{-18}	
	760 (1690)			
dtbpb	434 (3660)	1119	?	0.042(2)
	573 (1260)	{-60}		
	768 (2080)			

[a]Recorded in THF solution, at -80°C. [b]Values in parentheses are the shifts in peak position observed upon ^{18}O-labelling.

complexes and the observed isotope shifts ($\Delta\nu$ = 58 – 63 cm^{-1}) are consistent with assignment as such.[19-20] It should be noted that whereas the $[Cu^{II}(\eta^1\text{-}^{16}O_2^{\bullet-})(Ar_3\text{-}TMPA)]^+$ complexes produced with natural abundance O_2 exhibit a single ν(O-O) band, the $^{18}O_2$-labelled isotopologues of the Ar = dpb and dtbpb variants possess two readily resolved peaks of unequal intensity. The same may be true of the Ar = tpb complex, but the ^{18}O-labelled data is not of sufficient resolution to definitively determine whether this is the case or not. Regardless, observations of this type have precedence and are attributed to Fermi resonance with a non-enhanced vibrational mode.[23, 48]

The Cu-O stretching modes, ν(Cu-O), are also readily discerned in the resonance Raman spectra of the complexes. In the cases of $[Cu^{II}(\eta^1\text{-}O_2^{\bullet-})(tpb_3\text{-}TMPA)]^+$ and $[Cu^{II}(\eta^1\text{-}O_2^{\bullet-})(dpb_3\text{-}TMPA)]^+$ they present as Fermi doublets. Upon $^{18}O_2$ labelling, they shift to lower energy and appear as single bands. The situation is more complex for $[Cu^{II}(\eta^1\text{-}O_2^{\bullet-})(dtbpb_3\text{-}TMPA)]^+$ because several bands are observed in the both the natural abundance O_2 and $^{18}O_2$-labelled compounds (Figure S28). This is presumed to be, at least in part, due to Fermi resonance. However, the close-spacing of these features, combined with experimental error and limitations of the data, renders accurate assignment very difficult.

Quite remarkably, UV-Vis spectral features suggestive of trace formation of the complexes $[Cu^{II}(\eta^1\text{-}O_2^{\bullet-})(tpb_3\text{-}TMPA)]^+$ and $[Cu^{II}(\eta^1\text{-}O_2^{\bullet-})(dpb_3\text{-}TMPA)]^+$ are observed even at ambient temperatures (Figures 3b and 3c, plus Figures S20 and S21). Consistent with the entropically

disfavored nature of O_2 binding, these features increase in intensity at lower temperatures and by -40°C formation of the $Cu^{II}(\eta^1\text{-}O_2^{\bullet-})$ species are essentially complete. Reversal of these spectral changes can be achieved by increasing the temperature, which indicates that O_2 binding is reversible. The general oxygenation behavior of $[Cu^{I}(dtbpb_3\text{-}TMPA)(NCMe)]^+$ is similar to that of the tpb- and dpb-substituted systems. However, the onset of formation of $[Cu^{II}(\eta^1\text{-}O_2^{\bullet-})(dtbpb_3\text{-}TMPA)]^+$ occurs at a lower temperature, and it only becomes complete at ≤ -70°C (Figures 3c and S22). The reduced affinity of $[Cu^{I}(dtbpb_3\text{-}TMPA)(NCMe)]^+$ for O_2 binding is a consequence of the comparative instability of the +2 oxidation state of copper in this system. This is evident from the $E_{1/2}$ value of the $[Cu(Ar_3\text{-}TMPA)(NCMe)]^{2+/+}$ redox couple for Ar = dtbpb, which is 70 – 90 mV more positive than it is for Ar = dpb and tpb (see above).

Crucially, no spectral features associated with formation of higher nuclearity O_2 adducts, including $Cu^{II}(\mu^2\text{-}O_2^{2-})Cu^{II}$ complexes, are observed for any of the $[Cu^{II}(\eta^1\text{-}O_2^{\bullet-})(Ar_3\text{-}TMPA)]^+$ complexes, at any temperature. Furthermore, within a time frame of several hours, no evidence for self-decay of any of these three complexes was observed at temperatures ≤ -20°C. Above these temperatures, very slow decay does occur, possibly due to reaction with the solvent (or impurities therein), but the final products are presently unclear.

Reaction with phenolic substrates. THF was used as the solvent of choice in all of our reactivity studies and, in order to eliminate kinetic complications arising from pre-equilibrium binding of O_2, they were conducted at temperatures at which oxygenation of the $[Cu^{I}(Ar_3\text{-}TMPA)(NCMe)]^+$ complexes was essentially complete. As mentioned above, for Ar = dtbpb this is ≤ -70°C, whereas higher temperatures of ≤ -40°C are required for Ar = tpb and dpb. The impact of the differing steric profiles of our three $[Cu^{II}(\eta^1\text{-}O_2^{\bullet-})(Ar_3\text{-}TMPA)]^+$ complexes upon reaction with external substrates was, therefore, probed at -70°C. These studies were performed using 2,6-di-tert-butyl-4-methoxyphenol (MeO-ArOH) as a substrate because it has a comparatively weak O-H bond (bond dissociation energy (BDE) = 79.6 kcal mol^{-1})[52] and it is widely used in such studies, thereby allowing comparison with other published systems.

In all cases, addition of excess MeO-ArOH to the $[Cu^{II}(\eta^1\text{-}O_2^{\bullet-})(Ar_3\text{-}TMPA)]^+$ complexes led to first order loss of their chromophores (Figures 4a, S29, and S30). The observed rate constants (k_{obs}) were found to be linearly dependent upon substrate concentration (Figure 4b), thereby yielding the second order rate constants (k_2) listed in Table 2. Near identical k_2 values of 0.90(5) and 0.93(5) M^{-1} s^{-1} were measured for $[Cu^{II}(\eta^1\text{-}O_2^{\bullet-})(tpb_3\text{-}TMPA)]^+$ and $[Cu^{II}(\eta^1\text{-}O_2^{\bullet-})(dpb_3\text{-}TMPA)]^+$, but a more than 20-fold smaller value of 0.042(2) M^{-1} s^{-1} was obtained for $[Cu^{II}(\eta^1\text{-}O_2^{\bullet-})(dtbpb_3\text{-}TMPA)]^+$. Thus, it can be concluded that addition of a phenyl ring to the 4-position of the dpb substituent, to give tpb, has little impact upon reaction with the bulky MeO-ArOH substrate. Given that these Ph rings point away from the metal centre, even if they do increase the steric bulk projecting above the mean plane of the pyridine donor rings, this is not very surprising. In contrast, the *tert*-butyl groups in the dtbpb substituents might not be expected to impact substrate reactivity significantly because they project "laterally". However, it is clear from the X-ray structure of $[Cu^{II}(dtbpb_3\text{-}TMPA)(NCMe)]^{2+}$ that they crowd the incipient superoxo axial coordination site and we believe this is the origin of the suppressed reactivity of this system. Nevertheless, the low reactivity of $[Cu^{II}(\eta^1\text{-}O_2^{\bullet-})(dtbpb_3\text{-}TMPA)]^+$ limits the scope of reactivity studies that can be performed for it. Thus, it was decided that subsequent kinetic studies should focus upon $[Cu^{II}(\eta^1\text{-}O_2^{\bullet-})(tpb_3\text{-}TMPA)]^+$, which has near identical reactivity to $[Cu^{II}(\eta^1\text{-}O_2^{\bullet-})(dpb_3\text{-}TMPA)]^+$ but is easier to synthesize.

Reaction of the three $[Cu^{II}(\eta^1\text{-}O_2^{\bullet-})(Ar_3\text{-}TMPA)]^+$ complexes with MeO-ArOH, at -70°C, led to formation of similar charge transfer bands centered somewhere around 400 – 410 nm (Figures 4a, S29 and S30). Concomitantly, formation of a sharp feature at *ca.* 406 nm and a bump at *ca.* 390 nm is observed. These relatively sharp features correspond to the MeO-ArO$^{\bullet}$ phenoxyl radical.[53] The observation of phenoxyl radicals is indicative of formal transfer of a hydrogen atom to the superoxocopper(II) moiety. From this, it can be inferred that the 400 – 410 nm charge transfer bands formed during reaction with all three $[Cu^{II}(\eta^1\text{-}O_2^{\bullet-})(Ar_3\text{-}TMPA)]^+$ correspond to hydroperoxocopper(II) complexes, $[Cu^{II}(OOH)(Ar_3\text{-}TMPA)]^+$. Good agreement with the UV-Vis spectral features of previously reported hydroperoxocopper(II) complexes supports this supposition.[23, 48, 54-58] Furthermore, similar species could be obtained by addition of the H-atom donor TEMPO-H to $[Cu^{II}(\eta^1\text{-}O_2^{\bullet-})(tpb_3\text{-}TMPA)]^+$ (Figure S31) and by treatment of $[Cu^{II}(tpb_3\text{-}TMPA)(NCMe)]^{2+}$ with a combination of H_2O_2 and NEt_3 (Figure S32), both of which are standard methods for preparation of hydroperoxocopper(II) complexes.

The observed phenoxyl radical and $[Cu^{II}(OOH)(Ar_3\text{-}TMPA)]^+$ products can be obtained either through a hydrogen atom transfer (HAT) reaction or (in either order) a stepwise transfer of a proton and an electron (i.e., PT-ET or ET-PT). To probe these mechanistic possibilities, we sought to expand the range of phenolic substrates studied. However, the k_2 value measured for reaction of $[Cu^{II}(\eta^1\text{-}O_2^{\bullet-})(tpb_3\text{-}TMPA)]^+$ with MeO-ArOH, at -70°C, is (after taking temperature into account) 1 – 2 orders of magnitude lower than those reported for the analogous reaction with other TMPA-supported $Cu^{II}(\eta^1\text{-}O_2^{\bullet-})$ complexes (Table S10). Such sluggish reaction renders measurement of reaction kinetics with more oxidatively resistant phenols challenging at this temperature. Fortunately, the high stability of $[Cu^{II}(\eta^1\text{-}O_2^{\bullet-})(tpb_3\text{-}TMPA)]^+$ allows mitigation of this problem via study at higher temperatures.

The kinetic isotope effect (KIE) upon reaction of $[Cu^{II}(\eta^1\text{-}O_2^{\bullet-})(tpb_3\text{-}TMPA)]^+$ with MeO-ArOH was measured at -40°C. At this temperature, k_2 values of 7.8(4) and 0.69(3) M^{-1} s^{-1} were obtained for MeO-ArOH and its isotopomer MeO-ArOD (Figure 4c, Table 3), respectively, which equates to a KIE of 11.3(8). This confirms that the rate-determining step involves HAT or a proton transfer (PT). Similar KIEs were reported for reaction of $[Cu^{II}(\eta^1\text{-}O_2^{\bullet-})(DMM\text{-}TMPA)]^+$ with the same substrate (11),[46] and for reaction of the active oxidants of the enzymes PHM, DβM, and TβM (10 – 12),

Table 3. A summary of the second order rate constants (k_2, $M^{-1}\ s^{-1}$) measured for reaction of $[Cu^{II}(\eta^1\text{-}O_2^{\bullet-})(tpb_3\text{-}TMPA)]^+$ with various O-H, N-H and C-H bond substrates, in THF solution at -40°C. Where available, the reported pK_a values, oxidation potentials (E_{ox}, V *vs* Fc^+/Fc^0) and bond dissociation energies (BDEs, kcal mol^{-1}) of the substrates are listed.

	Substrate	k_2 ($M^{-1}\ s^{-1}$)	BDE (X-H) (kcal mol^{-1})	E_{ox} (V *vs* $Fc^{+/0}$)	pK_a
O-H substrates [a]	MeO-ArOH	7.8(4)	79.6	0.526	18.2
	MeO-ArOD	0.69(3)		0.585	
	MPPO-ArOH [b]	1.8(1)		0.614	
	CF_3CH_2O-ArOH	0.16(1)		0.805	
	Me-ArOH	0.086(4)	80.1	0.81	17.7
	Et-ArOH	0.053(3)	80.0	0.875	17.7
	^{t}Bu-ArOH	0.044(2)	82.3	0.927	17.8
N-H substrates [c]	DPH	25(1)	71.7		26.2
	DPH-d_2	1.3(1)			
	TPH	1.3(1)	83.5		24.5
	TPH-d	0.14(1)			
	Ph_2NH	0.00080(4)	89.9	0.455	25.0
C-H substrates [d]	BNAH	0.20(1)	70.7	0.219	
	BzImH	0.0099(5)	73.4	-0.179	

[a] BDE and pK_a values (in dmso) are taken from ref. [52], and the E_{ox} values (in MeCN) are taken from ref. [46]. [b] MPPO = 2-methyl-1-phenylpropan-2-yloxy. [c] With the exception of the k_2 values, data (measured in dmso) is taken from ref. [59]. [d] E_{ox} values and BDEs (in MeCN) are taken from ref [60].

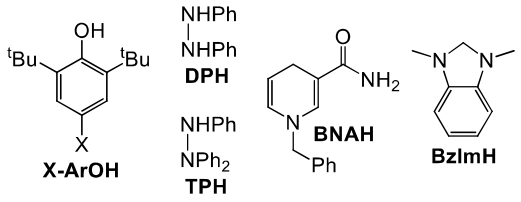

Chart 2. Substrates used in the reaction kinetics studies detailed herein.

which are evidenced to be $Cu^{II}(\eta^1\text{-}O_2^{\bullet-})$ intermediates.[11, 13-14] These published values were all presented as supporting evidence for HAT mechanisms.

In addition, we measured kinetics at -40°C for reaction of $[Cu^{II}(\eta^1\text{-}O_2^{\bullet-})(tpb_3\text{-}TMPA)]^+$ with several 2,6-di-tert-butylphenols possessing differing substituents (X) at the 4-position (X-ArOH, Scheme S4). Reaction was found, in all cases, to proceed with a first order dependence upon both complex and substrate, thereby yielding second order rate constants (Figures S33). The k_2 values obtained are summarized alongside reported BDE, E_{ox} and pK_a values, where available, in Table 3. The organic products of the reactions of $[Cu^{II}(\eta^1\text{-}O_2^{\bullet-})(tpb_3\text{-}TMPA)]^+$ with the X-ArOH substrates at -40°C were characterized upon warming to room temperature and, in all cases, approximately 0.5 equiv 2,6-di-tert-butyl-1,4-benzoquinone was obtained. This outcome has precedence and a mechanism explaining it, via initial generation of phenoxyl radicals, has been provided elsewhere.[46]

A Marcus-type plot of $(k_BT/e)\ln(k_2)$ versus oxidation potential (E_{ox}) of the phenols was constructed from the data obtained (Figure 4d).[30] It displays a good linear correlation and a best-fit line with a slope of -0.24 was obtained. The observation of a negative slope rules out a mechanism involving an initial discrete PT step. This is because the rate of a PT reaction would be expected to increase with decreasing pK_a and, given that the pK_a of phenols is inversely related with their E_{ox} values, a positive slope should result. The magnitude of the slope observed for $[Cu^{II}(\eta^1\text{-}O_2^{\bullet-})(tpb_3\text{-}TMPA)]^+$ is much larger than that reported for the cumylperoxyl radical (-0.05),[46, 61] which is accepted to react with phenols and (*N*,*N*-dimethylanilines) via "pure" HAT.[61-62] However, it is smaller than expected for a reaction involving an initial electron transfer and subsequent separate proton transfer step (-0.5 to -1.0).[61, 63-64] Instead, the observed correlation and slope is suggestive of a HAT reaction in which there is significant charge (electron) transfer.[65-66] A similar observation was reported for $[Cu^{II}(\eta^1\text{-}O_2^{\bullet-})(DMA\text{-}TMPA)]^+$, but a linear fit with a slightly larger gradient of -0.29 was obtained.[46] From this, it can be cautiously inferred that reaction of $[Cu^{II}(\eta^1\text{-}O_2^{\bullet-})(DMA\text{-}TMPA)]^+$ with phenols proceeds with greater charge transfer than $[Cu^{II}(\eta^1\text{-}O_2^{\bullet-})(tpb_3\text{-}TMPA)]^+$. One might expect this to manifest in differences in enthalpic barriers to reaction of these two complexes.

To further probe the oxidative potency of $[Cu^{II}(\eta^1\text{-}O_2^{\bullet-})(tpb_3\text{-}TMPA)]^+$, it was combined with the electron transfer agents ferrocene and decamethylferrocene (0.00 and -0.48 V, respectively, in MeCN solution)[67]. No reaction was observed in either case. This contrasts with $[Cu^{II}(\eta^1\text{-}O_2^{\bullet-})(L8)]^+$, which is able to react with both.[41] It is also

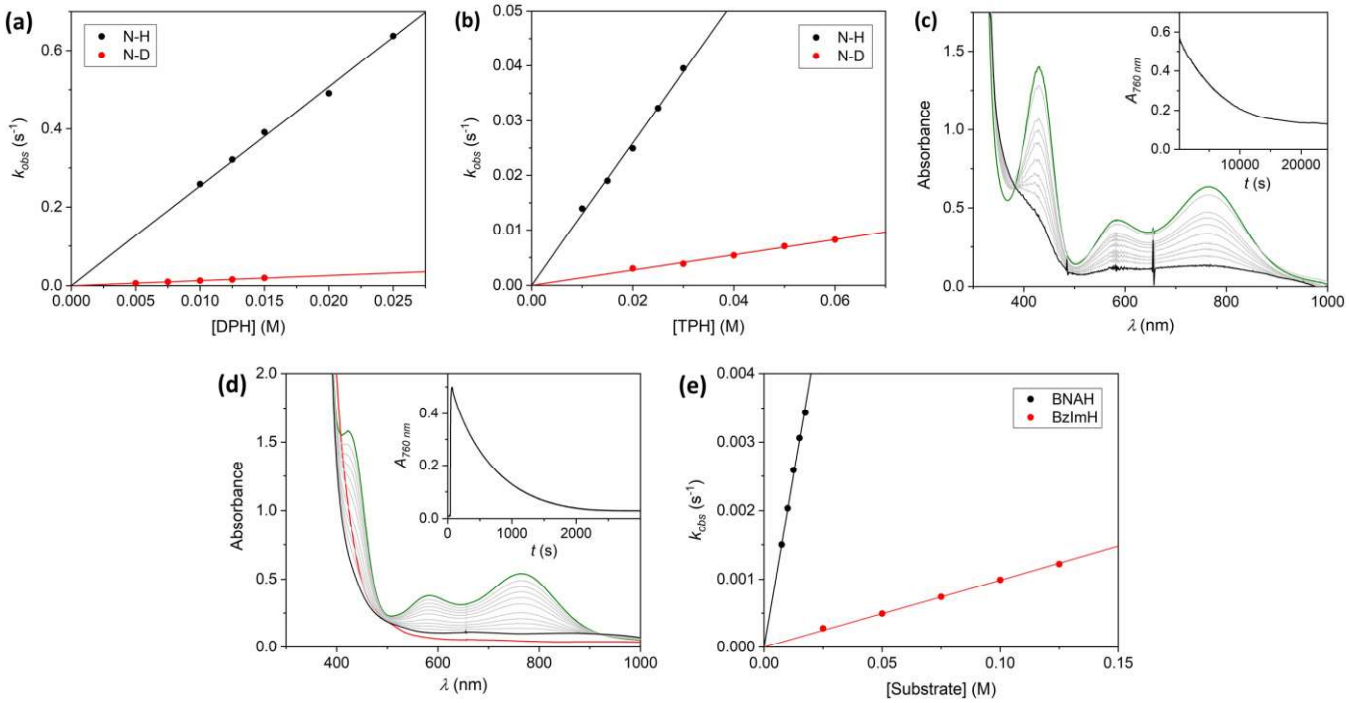

Figure 5. Plots of observed rate constants (k_{obs}, s^{-1}) versus substrate concentration (M) for reaction of $[Cu^{II}(\eta^1\text{-}O_2^{\bullet-})(tpb_3\text{-}TMPA)]^+$, in THF solution at -40°C, with: **(a)** DPH and its N-deuterated analogue, DPH-d_2 (black and red circles, respectively); and **(b)** TPH and its N-deuterated analogue, TPH-d (black and red circles, respectively). Reaction of $[Cu^{II}(\eta^1\text{-}O_2^{\bullet-})(tpb_3\text{-}TMPA)]^+$, in THF solution at -40°C, with the substrates **(c)** Ph_2NH and **(d)** BNAH. In the latter case, the substrate was added prior to oxygenation. **Main:** the starting copper(I) complex (not shown in **(c)**), superoxocopper(II) intermediate, product of reaction, and the spectra recorded during the course of reaction with the substrate are depicted using red, green, black, and grey lines, respectively. **Inset:** absorbance at 760 nm as a function of time. **(e)** Plot of observed rate constants (k_{obs}, s^{-1}) versus substrate concentration (M) for reaction of $[Cu^{II}(\eta^1\text{-}O_2^{\bullet-})(tpb_3\text{-}TMPA)]^+$, in THF solution at -40°C, with the C-H bond substrates BNAH and BzImH (black and red circles, respectively).

worth mentioning that although reaction was observed was upon addition of 2,6-di-tert-butylphenol (H-ArOH), it so slow that no efforts were made to measure reaction kinetics. This reflects the higher E_{ox} of this phenol (1.074 V) relative to the other X-ArOH substrates.[46] Given that H-ArOH also has a lower pK_a (17.3)[52] than the other X-ArOH substrates, it reinforces the inference that $[Cu^{II}(\eta^1\text{-}O_2^{\bullet-})(tpb_3\text{-}TMPA)]^+$ is also a comparatively weak base. These negative results reaffirm the conclusion that HAT is the mechanism by which this complex reacts with phenols.

Reaction with N-H and C-H substrates. In order to obtain a broader understanding of the reactivity of the $[Cu^{II}(\eta^1\text{-}O_2^{\bullet-})(Ar_3\text{-}TMPA)]^+$ complexes, we expanded our studies (at -40°C) to include N-H and C-H substrates. As with the phenolic substrates, reaction was found in all cases to be first order in both substrate and $Cu^{II}(\eta^1\text{-}O_2^{\bullet-})$ complex. Consistent with their respective relatively low BDEs of 71.7 and 83.5 kcal mol^{-1},[59] the substrates 1,2-diphenylhydrazine (DPH) and 1,1,2-triphenylhydrazine (TPH) are rapidly oxidized by $[Cu^{II}(\eta^1\text{-}O_2^{\bullet-})(tpb_3\text{-}TMPA)]^+$ (Figures 5a, 5b, S34, and S35). More specifically, k_2 values of 25(1) and 1.3(1) M^{-1} s^{-1} were measured for reaction with DPH and TPH, respectively. Subsequent room temperature work-up and analysis of the reaction mixtures confirmed that both substrates were oxidized by $2e^-$ to give ~1 equiv of product(s). In the case of DPH, this afforded azobenzene in 101(5) % yield (Eqn. S4, Table S7). However, oxidation of TPH proceeded via N-N bond cleavage and yielded nitrosobenzene and diphenylamine in yields of 108(9) and 113(9) % (Eqn. S5, Tables S8 and S9), respectively.

Reaction with the corresponding *N*-deuterated hydrazines DPH-d_2 and TPH-d proceeded with significantly reduced k_2 values (Figures 5a and 5b) of 1.3(1) and 0.14(1) M^{-1} s^{-1}, respectively. This equates to substantial KIEs of 19.8(14) for DPH and 9.4(7) for TPH. These values are comparable to (or larger than) that obtained for reaction with MeO-ArOH. Given that hydrazines are less acidic than phenols, these large KIEs can be attributed to HAT reactivity. In fact, the KIE for reaction with DPH is sufficiently large to imply H-atom tunnelling contributions.

In addition to hydrazines, we attempted reaction with the more challenging substrate diphenylamine (Ph_2NH), which possesses a relatively high N-H BDE of 89.9 kcal mol^{-1}.[59] It was successful, albeit very slow, and proceeded with a k_2 value of $8.0(4) \times 10^{-4}$ M^{-1} s^{-1} (Figures 5c and S36). Given that the E_{ox} of diphenylamine (0.455 V) is much higher than that of decamethylferrocene and its pK_a (25.0) is significantly higher than the 4-substituted-2,6-di-tert-butylphenols used in this study, reaction via an initial H^+ or e^- transfer can be ruled out. Instead, oxidation by HAT is most likely.

Oxidation of C-H bond substrates proved to be a more challenging proposition. One difficulty arose from the

coordinating nature of the olefinic functional groups found in many substrates containing activated C-H bonds. This allows them to compete with O_2 in binding to the copper(I) starting complex $[Cu^{I}(tpb_3\text{-}TMPA)(NCMe)]^+$. Consequently, addition of such substrates to $[Cu^{II}(\eta^1\text{-}O_2^{\bullet-})(tpb_3\text{-}TMPA)]^+$ causes an initial drop in the concentration of this complex due to partial reversal of O_2 binding and formation of $[Cu^{I}(tpb_3\text{-}TMPA)(olefin)]^+$ complexes. This is graphically demonstrated by sequential addition of multiple portions of 1,4-cyclohexadiene (CHD) to $[Cu^{II}(\eta^1\text{-}O_2^{\bullet-})(tpb_3\text{-}TMPA)]^+$ (Figure S37). Oxidation of this substrate is extremely sluggish and the CHD portions only cause stepwise incremental decreases in $Cu^{II}(\eta^1\text{-}O_2^{\bullet-})$ concentration. Although this ligand metathesis process is much more rapid than substrate oxidation for the C-H bond substrates studied, it does complicate simulation of reaction kinetics. Thankfully, this problem can be circumvented by adding substrate to the copper(I) starting complex prior to oxygenation, which results in a clean first order reaction with $[Cu^{II}(\eta^1\text{-}O_2^{\bullet-})(tpb_3\text{-}TMPA)]^+$ (Figures 5d and S38).

Reaction with 1-benzyl-1,4-dihydronicotinamide (BNAH) and 1,3-dimethyl-2,3-dihydrobenzimidazole (BzImH), which have very low C-H BDEs of 70.7 and 73.4 kcal mol^{-1},[60] afforded ~1 equiv of their 2e$^-$ oxidized products 1-benzylnicotinamidium (BNA^+) and 1,3-dimethylbenzimidazolium ($BzIm^+$) after work-up (Eqns. S1 and S3, Tables S5 and S6). In addition to being H-atom donors, these reagents are also potential hydride donors. However, their relative tendencies to function as hydride donors (64.2 kcal mol^{-1} for BNAH and 49.5 kcal mol^{-1} for BzImH)[60] is the opposite of their H-atom donor abilities. More specifically, BNAH is more reactive than BzImH as a H-atom donor, but weaker as a H$^-$ donor. Given that $[Cu^{II}(\eta^1\text{-}O_2^{\bullet-})(tpb_3\text{-}TMPA)]^+$ reacts with BNAH 20 times more quickly than with BzImH (Figure 5e, k_2 values of 0.20(1) and 0.0099(5) M^{-1} s^{-1}, respectively), it can be concluded that reaction proceeds via HAT. This outcome mirrors that previously reported for $[Cu^{II}(\eta^1\text{-}O_2^{\bullet-})(^{(Piv)}TMPA)]^+$, which reacts 2.4 times more quickly with BNAH than it does with BzImH.[47]

The rates measured for reaction of $[Cu^{II}(\eta^1\text{-}O_2^{\bullet-})(tpb_3\text{-}TMPA)]^+$ with BNAH and BzImH are significantly lower than those measured for reaction with MeO-ArOH and TPH, despite the latter substrates possessing O-H and N-H bonds that are significantly stronger than the C-H bonds of the former (Table 3). Indeed, attempts to measure reaction kinetics for the substrates xanthene and 9,10-dihydroanthracene, which have slightly higher C-H BDEs (77.9 and 80.6 kcal mol^{-1}, respectively)[59] were unsuccessful, with no kinetically measurable reaction being observed at -40°C. This implies factors beyond simple thermodynamic considerations are important in controlling reactivity.

It has long been known that HAA from C-H bonds is very slow relative to reaction with O-H and N-H bonds.[68-69] This has been rationalized using the Marcus cross relation:[70-72]

$$k_{AH/B} = \sqrt{k_{AH/A}k_{BH/B}K_{eq}f}$$

where K_{eq} is the equilibrium constant for the HAT in question, which equates to the thermodynamic driving force for the reaction, $k_{AH/A}$ and $k_{BH/B}$ are H-atom self-exchange rate constants, and f is the frequency factor, which is usually assumed to be close to 1.[73] In our case, $k_{AH/A}$ is associated with self-exchange between $[Cu^{II}(\eta^1\text{-}O_2^{\bullet-})(tpb_3\text{-}TMPA)]^+$ and the corresponding $Cu^{II}(\eta^1\text{-}OOH)$ complex, and $k_{BH/B}$ is for the reacting substrate bond (X-H) and the immediate product of HAA ($X^{\bullet}$). For reactions of $[Cu^{II}(\eta^1\text{-}O_2^{\bullet-})(tpb_3\text{-}TMPA)]^+$ with C-H and N/O-H bonds possessing identical DBFEs (i.e., identical K_{eq} values), the rate is dependent upon the respective $k_{BH/B}$ values of the substrates. Rates of self-exchange for C-H bond substrates tend to be several orders of magnitude smaller than those for O-H and N-H bonds.[72, 74] Thus, reaction with C-H bonds is expected and experimentally observed to be inherently slower.

Activation parameters. The high stability of $[Cu^{II}(\eta^1\text{-}O_2^{\bullet-})(tpb_3\text{-}TMPA)]^+$ against formation of higher nuclearity species allows for measurement of kinetic data over a broad temperature range, which provides an opportunity to access more detailed mechanistic information. To exploit this, we have measured k_2 values for reaction with selected substrates at regular increments over temperature ranges of -40 to -90°C (Figures S39 – S44, Tables S11 – S14). Given how sluggish reaction is at lower temperatures, these studies are limited to the easily oxidized substrates MeO-ArOH, DPH, TPH and BNAH. Linear fits of the Eyring plots constructed using this data (Figure 6a) yields the enthalpic ($\Delta H^{\ddagger}$) and entropic ($\Delta S^{\ddagger}$) barriers to reaction listed in Table 4.

The most prominent feature of the activation parameters measured for reaction of $[Cu^{II}(\eta^1\text{-}O_2^{\bullet-})(tpb_3\text{-}TMPA)]^+$ with the substrates MeO-ArOH, DPH, TPH and BNAH are the large entropic barriers to reaction. This is characteristic of (bimolecular) HAT reactions and reflects a high degree of preorganization of their transition states. The $\Delta S^{\ddagger}$ measured for reaction with BNAH, at -33 ± 0.7 cal mol^{-1} K^{-1}, is the largest amongst the substrates studied. However, the difference with the entropic barriers for reaction with the other substrates is not enormous, and the sluggish reaction with BNAH is also contributed to by the comparatively large $\Delta H^{\ddagger}$ of 6.7 ± 0.2 kcal mol^{-1} associated with this substrate.

Thus far, few measurements have been made of Eyring parameters for HAT reactions between $Cu^{II}(\eta^1\text{-}O_2^{\bullet-})$ complexes and substrates. One of the few reports is for reaction of $[Cu^{II}(\eta^1\text{-}O_2^{\bullet-})(DMA\text{-}TMPA)]^+$ with MeO-ArOH, where $\Delta H^{\ddagger}$ and $\Delta S^{\ddagger}$ values of 3.6 ± 0.6 kcal mol^{-1} and -32 ± 3 cal mol^{-1} K^{-1} were obtained.[46] Another example is reaction of Meyer's pyrazolate-bridged $Cu^{II}(\eta^1\text{-}O_2^{\bullet-})Cu^{II}$ complex with TEMPO-H, which was accompanied by $\Delta H^{\ddagger}$ and $\Delta S^{\ddagger}$ values of 9.0 ± 0.4 kcal mol^{-1} and -26.8 ± 1.7 cal mol^{-1} K^{-1}, respectively.[75] The $\Delta S^{\ddagger}$ values for the two aforementioned systems are quite similar to that measured for reaction of $[Cu^{II}(\eta^1\text{-}O_2^{\bullet-})(tpb_3\text{-}TMPA)]^+$ with MeO-ArOH (-28 ± 0.6 cal mol^{-1} K^{-1}). Instead, the major difference between the activation parameters for these three reactions with O-H bonds is the magnitude of their respective $\Delta H^{\ddagger}$ values. The most reactive system, $[Cu^{II}(\eta^1\text{-}O_2^{\bullet-})(DMA\text{-}TMPA)]^+$, has the lowest enthalpic barrier to reaction and the least reactive, the $Cu^{II}(\eta^1\text{-}O_2^{\bullet-})Cu^{II}$ complex, has the largest. The $\Delta H^{\ddagger}$ of 6.1 ± 0.1 kcal mol^{-1} measured for $[Cu^{II}(\eta^1\text{-}O_2^{\bullet-})(tpb_3\text{-}TMPA)]^+$ is intermediate in size. Although other factors may contribute, it is likely that the differences in reactivity of these superoxocopper(II) complexes is correlated with their relative thermodynamic

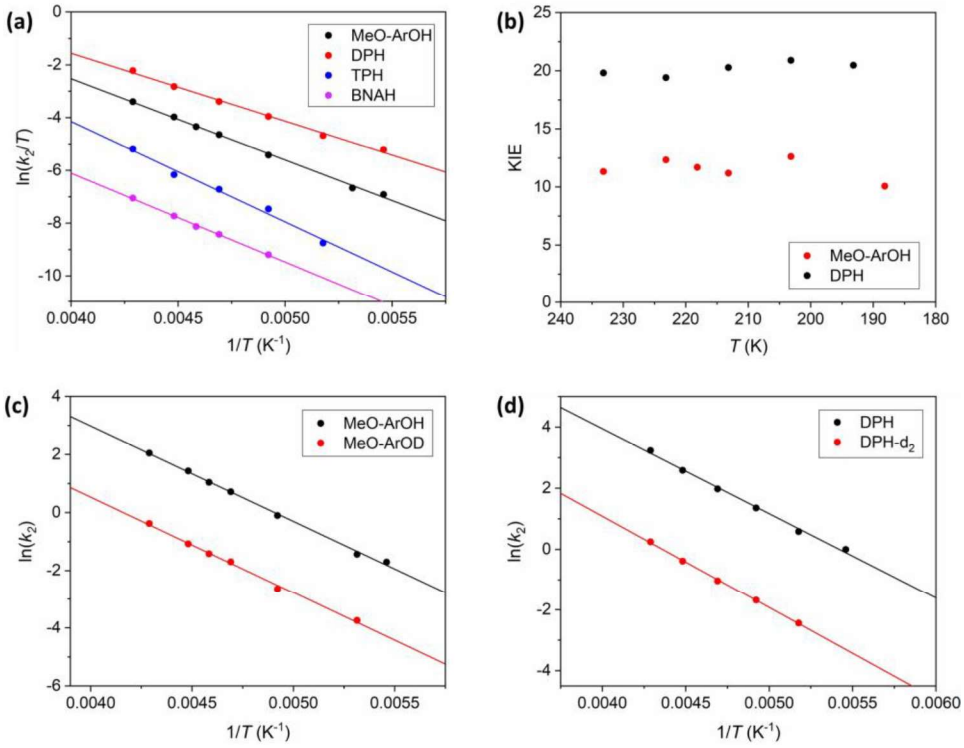

Figure 6. (a) Eyring plots for reaction of $[Cu^{II}(\eta^1\text{-}O_2^{\bullet-})(tpb_3\text{-}TMPA)]^+$ with the substrates MeO-ArOH, DPH, TPH, and BNAH (black, red, blue and magenta cirlces, respectively). **(b)** Kinetic isotope effects (KIEs) upon reaction of $[Cu^{II}(\eta^1\text{-}O_2^{\bullet-})(tpb_3\text{-}TMPA)]^+$ with MeO-ArOH and DPH (red and black circles, respectively) versus temperature (*T*, K). The KIE values used to construct the plot are listed in Tables S11 and S12. Arrhenius plots for reaction of $[Cu^{II}(\eta^1\text{-}O_2^{\bullet-})(tpb_3\text{-}TMPA)]^+$ with: **(c)** MeO-ArOH and MeO-ArOD (black and red ricles, respectively); and **(d)** DPH and DPH-d_2 (black and red circles, respectively). Plots of k_{obs} versus substrate concentration, as a function of temperature, used to construct **(a – d)** appear in the Supporting Information (Figures S39 – S44). The second order constants derived therefrom are listed in Tables S11 – S14, and the values from fitting the Arrhenius plots are listed in Table S15.

driving forces for reaction (i.e., the strength of the $Cu^{II}OO$-H bonds formed). This may be related to our above suggestion of greater charge transfer in the HAT reactivity of $[Cu^{II}(\eta^1\text{-}O_2^{\bullet-})(DMM\text{-}TMPA)]^+$ with X-ArOH substrates relative to $[Cu^{II}(\eta^1\text{-}O_2^{\bullet-})(tpb_3\text{-}TMPA)]^+$.

Eyring parameters have been reported for reaction of the superoxocobalt(III) complex $[Co^{III}(\eta^1\text{-}O_2^{\bullet-})(py)(TBP_8Cz)]^-$ with DPH. These $\Delta H^{\ddagger}$ and $\Delta S^{\ddagger}$ values, of 6.7 ± 0.1 kcal mol^{-1} and -23 ± 0.4 cal mol^{-1} K^{-1},[76] are respectively larger and smaller than those measured for $[Cu^{II}(\eta^1\text{-}O_2^{\bullet-})(tpb_3\text{-}TMPA)]^+$ (5.1 ± 0.2 kcal mol^{-1} and -30 ± 0.9 cal mol^{-1} K^{-1}, respectively). Within the temperature window of study, these two factors counterbalance each other, and the two complexes display similar rates of reaction. TPH has a stronger N-H bond than DPH and, as a consequence, the enthalpic barrier to reaction of the former substrate with $[Cu^{II}(\eta^1\text{-}O_2^{\bullet-})(tpb_3\text{-}TMPA)]^+$ is significantly larger (7.6 ± 0.5 kcal mol^{-1}) and reaction is slower.

Concordant with the kinetically inert nature of C-H bonds, there are very few reports of activation parameters for reaction of C-H bond substrates with $Cu^{II}(\eta^1\text{-}O_2^{\bullet-})$ complexes. Indeed, the values reported for intramolecular self-hydroxylation in $[Cu^{II}(\eta^1\text{-}O_2^{\bullet-})(L8)]^+$ represents the best point of comparison for those obtained from reaction of $[Cu^{II}(\eta^1\text{-}O_2^{\bullet-})(tpb_3\text{-}TMPA)]^+$ with BNAH. The entropic barrier to self-hydroxylation in the former is very large (-53 ± 0.1 cal mol^{-1} K^{-1}), much larger than the latter, intermolecular reaction (-33 ± 0.7 cal mol^{-1} K^{-1}). This implies that the transition state for self-decay of $[Cu^{II}(\eta^1\text{-}O_2^{\bullet-})(L8)]^+$ has particularly severe geometric restrictions. Without knowing the thermodynamic driving forces for these reactions, further insight is difficult. Correspondingly, it is difficult to make direct comparisons with other complexes when different substrates have been employed, such as Tolman's hydroxocopper(III) complexes, whose activation parameters vary quite significantly upon modification of the supporting ligand. To allow more meaningful conclusions to be drawn, a much larger survey of Eyring parameters for reaction of $Cu^{II}(\eta^1\text{-}O_2^{\bullet-})$ complexes with substrates is required.

Temperature dependence of KIEs. Kinetic isotope effect (KIE) measurements can be highly informative and allow inferences to be drawn about reaction mechanism. For instance, HAT reactions are frequently marked by large KIE values, with H-atom tunnelling being suggested for values that far exceed semi-classical limits. However, assessment on this basis alone can sometimes lead to incorrect elimination of tunnelling as a mechanism, and it has been shown that more robust information can be obtained from

Table 4. Activation enthalpies and entropies ($\Delta H^{\ddagger}$ and $\Delta S^{\ddagger}$, respectively) obtained from Eyring plots for reaction of $[Cu^{II}(\eta^1\text{-}O_2^{\bullet-})(tpb_3\text{-}TMPA)]^+$ with substrates, plus differences between the activation energies for reaction with protio substrates and their deuterated congeners ($\Delta E_A = E_a(H) - E_a(D)$) and ratios of the associated collision frequencies (A_H/A_D) calculated from Arrhenius plots. For comparison, values for selected published complexes are included.

Complex	Substrate	$\Delta H^{\ddagger}$ (kcal mol^{-1})	$\Delta S^{\ddagger}$ (cal mol^{-1} K^{-1})	ΔE_A (kcal mol^{-1})	A_H/A_D
$[Cu^{II}(\eta^1\text{-}O_2^{\bullet-})(tpb_3\text{-}TMPA)]^+$	MeO-ArOH	6.1 ± 0.1	-28 ± 0.6	0.034	11
	DPH	5.1 ± 0.2	-30 ± 0.9	0.45	7.1
	TPH	7.6 ± 0.5	-25 ± 2.4		
	BNAH	6.7 ± 0.2	-33 ± 0.7		
$[Cu^{II}(\eta^1\text{-}O_2^{\bullet-})(DMM\text{-}TMPA)]^+$ [46]	MeO-ArOH	3.6 ± 0.6	-32 ± 3		
$[Cu^{II}(\eta^1\text{-}O_2^{\bullet-})(L8)]^+$ [43]	benzylic CH_2	4.5 ± 0.02	-53 ± 0.1		
$Cu^{II}(1,2\text{-}\mu\text{-}O_2^{\bullet-})Cu^{II}$ [75]	TEMPO-H	9.0 ± 0.4	-27 ± 1.7		
$[Cu^{III}(OH)(L)]^-$ [77-78]	DHA	5.1(1)	-31(3)	0.3	13
$[Cu^{III}(OH)(^{NO2}L)]^-$ [77]	DHA	4.9(1)	-27(1)	3.0	0.05
$[Cu^{III}(OH)(^{pipMe}L)]^-$ [77]	DHA	3.8(2)	-38(3)	3.6	0.01
$[Co^{III}(\eta^1\text{-}O_2^{\bullet-})(py)(TBP_8Cz)]^-$ [76]	DPH	6.7 ± 0.1	-23 ± 0.4		
$[Cr^{III}(\eta^1\text{-}O_2^{\bullet-})(Cl)(TMC)]^+$ [79]	$AcrH_2$			10.8	4.1×10^{-8}
PHM[15]	Hippuric acid			0.37	5.9
WT-SLO[80]	Linoleic acid			0.9	18

temperature-dependent KIE measurements, and the Arrhenius parameters derived therefrom.[81-83] More specifically, from the ratio of the collision factors for reaction with the protio and deuterio substrates (A_H/A_D) and differences in the associated activation energies ($\Delta E_a = E_a(H) - E_a(D)$). Such variable temperature KIE studies have proven to be very revealing in enzymatic studies. However, they are seldom performed for model complexes and, other than inconclusive measurements for $[Cu^{II}(\eta^1\text{-}O_2^{\bullet-})(DMA\text{-}TMPA)]^+$ (due to the very limited temperature range studied),[46] we are unaware of any examples for superoxocopper(II) model complexes.

For a semi-classical HAT reaction, A_H/A_D should equal 1 ($\Delta E_a > 0$), with KIE values arising from differences in zero-point energies. Models with corrections for H-atom tunnelling through the reaction barrier are characterized by $A_H/A_D < 1$ and $\Delta E_a >> 0$. This can give rise to highly temperature sensitive KIEs, with very large values often being seen at low temperatures. Reaction of the complexes $[Cu^{III}(OH)(^{NO2}L)]^-$ and $[Cu^{III}(OH)(^{pipMe}L)]^-$ with DHA, reported by Tolman and co-workers,[77] and reaction of $[Cr^{III}(\eta^1\text{-}O_2^{\bullet-})(Cl)(TMC)]^+$ with $AcrH_2$, reported by Nam and co-workers,[79, 84] both adhere to this paradigm. In particular, the latter proceeds with a KIE of 74 ± 5 at -20°C that increases to a remarkably large value of 470 ± 30 at -40°C.[79] Correspondingly, the ΔE_a of 10.8 kcal mol^{-1} and A_H/A_D of only 4.1×10^{-8}, respectively, measured for this system deviate greatly from semi-classical values.

A third scenario involving extensive tunnelling of both H- and D-atoms yields temperature independent KIE values, which equate to $A_H/A_D > 1$ and near-zero ΔE_a values. This type of behaviour has been observed at physiological temperatures in wild-type enzymes, where HAT donor-acceptor distances can be optimized by the secondary structure of the enzyme active site. For instance, in Peptidylglycine α-Amidating Monoxygenase and Soybean Lipoxygenase (A_H/A_D = 5.9 and 18, respectively)[15, 80], wherein their respective end-on superoxocopper(II) and hydroxoiron(III) active oxidants are responsible for substrate C-H bond oxidation. However, model complexes tend to show this type of behaviour only at low temperatures. For example, reaction of Tolman's hydroxocopper(III) complex $[Cu^{III}(OH)(L)]^-$ with DHA (from -20 to -80°C) is accompanied by a large A_H/A_D of 13 and a ΔE_a of only 0.3 kcal mol^{-1}.[77-78] This diverges significantly from the temperature dependence of the KIEs measured for its derivatives $[Cu^{III}(OH)(^{NO2}L)]^-$ and $[Cu^{III}(OH)(^{pipMe}L)]^-$.

For $[Cu^{II}(\eta^1\text{-}O_2^{\bullet-})(tpb_3\text{-}TMPA)]^+$, KIE measurements over a reasonably large temperature range are only feasible for the most reactive substrates, MeO-ArOH and DPH. In both cases, the KIE values are essentially temperature independent between -40 and -90°C (Figure 6b), with those of MeO-ArOH and DPH falling within the ranges 10.1(7) – 12.6(9) and 19.4(14) – 20.9(15), respectively. This is readily apparent from the quasi-parallel nature of the best fit lines in the Arrhenius plots constructed for the substrates MeO-ArOH and MeO-ArOD, and DPH and DPH-d_2 (Figures 6c and 6d). The ΔE_a and A_H/A_D values derived from these plots are listed in Table 4. Consistent with the preceding assertions, respective ΔE_a and A_H/A_D values of 0.034 kcal mol^{-1} and 11 were obtained for MeO-ArOH and MeO-ArOD. Corresponding values of 0.45 kcal mol^{-1} and 7.1 were obtained for DPH and DPH-d_2. On this basis, we can conclude that the HAT reactions between $[Cu^{II}(\eta^1\text{-}O_2^{\bullet-})(tpb_3\text{-}TMPA)]^+$ and these substrates, which possess weak O-H and N-H bonds, proceeds via tunnelling of both H- and D-atoms.

CONCLUSION

In this study, we have shown that installation of bulky aryl substituents at the 5-position of the pyridyl rings of the TMPA ligand provides copper(I) complexes, $[Cu^{I}(Ar_3\text{-}TMPA)(NCMe)]^{+}$ (Ar = tpb, dph, dtbpb), that undergo reversible oxygenation to yield the corresponding $[Cu^{II}(\eta^1\text{-}O_2^{\bullet-})(Ar_3\text{-}TMPA)]^{+}$ complexes. Crucially, no conversion to higher nuclearity species, such as $Cu^{II}(\mu^2\text{-}O_2^{2-})Cu^{II}$ complexes, was observed under any of the experimental conditions studied. As can be seen from X-ray crystal structures of $[Cu^{II}(Ar_3\text{-}TMPA)(NCMe)]^{2+}$, the aryl substituents point away from the metal centre and the majority of their bulk projects perpendicular to the plane of the pyridine rings. This increases the effective cone angle of the donors and prohibits the interdigitation of donors, which is a pre-requisite of dinuclear complex formation.

Consistent with its entropically disfavored nature, the extent of O_2 binding increases with decreasing temperature, and it can be reversed by warming to ambient temperatures. Oxygenation for Ar = tpb and dpb is essentially complete by -40°C and traces of their $[Cu^{II}(\eta^1\text{-}O_2^{\bullet-})(Ar_3\text{-}TMPA)]^{+}$ complexes can even be observed at room temperature. However, lower temperatures of ~0°C are required for commencement of O_2 binding by Ar = dtbpb and it becomes complete at *ca.* -70°C. This reduced affinity for O_2 is because the "lateral" steric bulk of the Ar = dtbpb substituents is so large that it impinges upon the metal centre. This weakens the donor strength of the ligand, which increases the $E_{1/2}$ of the $[Cu(dtbpb_3\text{-}TMPA)(NCMe)]^{2+/+}$ redox couple relative to the Ar = tpb and dpb complexes, thereby decreasing the driving force for binding O_2. Regardless, the non-traditional employment of steric bulk used in this study provides $Cu^{II}(\eta^1\text{-}O_2^{\bullet-})$ complexes that are fully stable against collapse to the corresponding $Cu^{II}(\mu^2\text{-}O_2^{2-})Cu^{II}$ species. Oxygenation behavior and high $Cu^{II}(\eta^1\text{-}O_2^{\bullet-})$ stability of this type has been previously reported only for Schindler's complex $[Cu^{II}(\eta^1\text{-}O_2^{\bullet-})(TMG_3\text{-}tren)]^{+}$.[32-33, 85] However, unlike $[Cu^{II}(\eta^1\text{-}O_2^{\bullet-})(TMG_3\text{-}tren)]^{+}$, our $[Cu^{II}(\eta^1\text{-}O_2^{\bullet-})(Ar_3\text{-}TMPA)]^{+}$ systems display significant reactivity with external substrates.

Although the steric bulk of the aryl substituents in $[Cu^{II}(\eta^1\text{-}O_2^{\bullet-})(Ar_3\text{-}TMPA)]^{+}$ is mostly directed away from the metal centre, it does have an impact upon reaction with substrates. This is readily apparent from the sluggish reactivity of the Ar = dtbpb complex relative to its Ar = tpb and dpb analogues, and it is likely the origin of the low reactivity of the $[Cu^{II}(\eta^1\text{-}O_2^{\bullet-})(Ar_3\text{-}TMPA)]^{+}$ complexes compared with previously published TMPA derivatives. Eyring measurements and Marcus plots of E_{ox} *vs* k_2 suggest that this may have an enthalpic origin but, at present, it is not clear how this arises from the steric bulk of the Ar substituents. Nonetheless, the high stability of our $[Cu^{II}(\eta^1\text{-}O_2^{\bullet-})(Ar_3\text{-}TMPA)]^{+}$ complexes allows us to compensate for this deficiency by performing reactivity studies at higher temperatures.

We have exploited the aforementioned appealing properties by examining the reaction of $[Cu^{II}(\eta^1\text{-}O_2^{\bullet-})(tpb_3\text{-}TMPA)]^{+}$ with a wide range of O-H, N-H and C-H bond substrates. In all cases reaction was found to proceed via HAT. Evidence for this includes large KIEs for reaction with MeO-ArOH, DPH and TPH (11.3(8), 19.8(14) and 9.4(7), respectively, at -40°C); an inability to react with simple electron transfer agents and weak acids; and a "Marcus plot" derived from reaction with a series of 4-substituted 2,6-di-tert-butylphenols (X-ArOH) possessing a negative slope of -0.24, which implies a HAT reaction that proceeds with significant charge transfer. The ease of oxidation of MeO-ArOH and DPH allowed measurement of KIEs over a 50°C temperature window (from -40 to -90°C). They were found to be effectively constant, with the resulting Arrhenius parameters ($A_H/A_D >> 1$ and $\Delta E_A \sim 0$) indicating that HAT reaction (for these substrates) proceeds via tunneling of both H and D atoms.

As anticipated, based upon previous precedent and the Marcus cross relation, oxidation of C-H bonds proved to be very challenging relative to O-H and N-H bonds. More specifically, $[Cu^{II}(\eta^1\text{-}O_2^{\bullet-})(tpb_3\text{-}TMPA)]^{+}$ is kinetically competent for reaction with diphenylamine (BDE = 89.9 kcal mol^{-1}), which possesses a moderately strong N-H bond, but is only able to oxidize substrates containing very weak C-H bonds. Thus, although the rates at which $[Cu^{II}(\eta^1\text{-}O_2^{\bullet-})(tpb_3\text{-}TMPA)]^{+}$ reacts with substrates is inversely correlated with the X-H BDEs of the substrates, it is clear that this is not the sole determining factor. Efforts to correlate these observed general trends in reactivity to kinetic barriers (derived from Eyring plots) for reaction with the substrates MeO-ArOH, DPH, TPH, and BNAH did not yield a simple answer. Although the entropy of activation for reaction with BNAH is larger than for the other substrates, the difference is not sufficient to fully explain the observed reactivity differences, and a relatively large enthalpic barrier is also a contributing factor. Attempts to draw broader and more insightful conclusions are handicapped by the dearth of reports of Eyring parameters for HAT reactions to superoxocopper(II) complexes (or related late transition superoxometal complexes), and it is clear that a more extensive survey of such data would be greatly beneficial.

In summary, we have developed a handful of remarkably stable $Cu^{II}(\eta^1\text{-}O_2^{\bullet-})$ complexes that retain significant reactivity with substrates. This has allowed us to conduct extensive reactivity studies, including rare examples of variable temperature studies. The results obtained provide insight into the inherent reactivity properties of the $Cu^{II}(\eta^1\text{-}O_2^{\bullet-})$ species. Unfortunately, oxidation of moderate-to-high strength C-H bonds remains a serious challenge and emulation of the hydroxylation chemistry displayed by the non-coupled dinuclear copper enzymes continues to be elusive. The prearrangement and activation of substrates by the secondary structure of the enzymes likely plays a major role in facilitating such chemistry. Nevertheless, we believe that there is scope for (and we are working on) enhancing the reactivity of our $[Cu^{II}(\eta^1\text{-}O_2^{\bullet-})(Ar_3\text{-}TMPA)]^{+}$ systems via modulation of the ligand steric bulk, which clearly hinders reaction, and moving to higher temperatures, where O_2 binding is less favored but substrate oxidation is more facile.

ASSOCIATED CONTENT

Supporting Information. Experimental and synthetic procedures, X-ray crystallographic data collection and structural parameters, additional UV-Vis and resonance Raman spectra, and reaction kinetics data (PDF).
Crystal structures of copper(II) complexes (CIF).

This material is available free of charge via the Internet at http://pubs.acs.org.

AUTHOR INFORMATION

Corresponding Author

* Email: jengland@ntu.edu.sg.

Author Contributions

‡These authors contributed equally.

Notes

The authors declare no competing financial interest. CIF data for associated crystal structures have been deposited in the Cambridge Crystallographic Data Centre under deposition numbers CCDC 1959106, 2094618, and 2094668.

ACKNOWLEDGMENT

JE is grateful to NTU (M4081442, 000416-00001) and the Ministry of Education of Singapore (AcRF Tier 1 grant RG8/19 (S), 002689-00001) for funding. We thank Dr. Rakesh Ganguly and Dr. Yongxin Li of the SPMS (NTU) X-ray lab for measurement and refinement of X-ray crystallographic data. In addition, we thank Ms. Anchisar Rakthanyakan for help with collecting Resonance Raman data.

REFERENCES

(1) Solomon, E. I.; Heppner, D. E.; Johnston, E. M.; Ginsbach, J. W.; Cirera, J.; Qayyum, M.; Kieber-Emmons, M. T.; Kjaergaard, C. H.; Hadt, R. G.; Tian, L. Copper Active Sites in Biology. *Chem. Rev.* **2014**, *114*, 3659-3853.

(2) Quist, D. A.; Diaz, D. E.; Liu, J. J.; Karlin, K. D. Activation of dioxygen by copper metalloproteins and insights from model complexes. *J. Biol. Inorg. Chem.* **2017**, *22*, 253-288.

(3) Whittaker, J. W. Free Radical Catalysis by Galactose Oxidase. *Chem. Rev.* **2003**, *103*, 2347-2364.

(4) Whittaker, M. M.; Whittaker, J. W. Catalytic Reaction Profile for Alcohol Oxidation by Galactose Oxidase. *Biochemistry* **2001**, *40*, 7140-7148.

(5) Whittaker, J. W. Galactose oxidase. In *Advances in Protein Chemistry*, Academic Press: 2002; Vol. 60, pp 1-49.

(6) Klinman, J. P. Mechanisms Whereby Mononuclear Copper Proteins Functionalize Organic Substrates. *Chem. Rev.* **1996**, *96*, 2541-2561.

(7) Klinman, J. P. The Copper-Enzyme Family of Dopamine β-Monooxygenase and Peptidylglycine α-Hydroxylating Monooxygenase: Resolving the Chemical Pathway for Substrate Hydroxylation. *J. Biol. Chem.* **2006,** *281*, 3013-3016.

(8) Appel, M. J.; Meier, K. K.; Lafrance-Vanasse, J.; Lim, H.; Tsai, C.-L.; Hedman, B.; Hodgson, K. O.; Tainer, J. A.; Solomon, E. I.; Bertozzi, C. R. Formylglycine-generating enzyme binds substrate directly at a mononuclear Cu(I) center to initiate O_2 activation. *Proc. Natl. Acad. Sci. U.S.A.* **2019**, *116*, 5370-5375.

(9) Miarzlou, D. A.; Leisinger, F.; Joss, D.; Häussinger, D.; Seebeck, F. P. Structure of formylglycine-generating enzyme in complex with copper and a substrate reveals an acidic pocket for binding and activation of molecular oxygen. *Chem. Sci.* **2019**, *10*, 7049-7058.

(10) Evans, J. P.; Ahn, K.; Klinman, J. P. Evidence That Dioxygen and Substrate Activation Are Tightly Coupled in Dopamine β-Monooxygenase: Implications for the Reactive Oxygen Species. *J. Biol. Chem.* **2003**, *278*, 49691-49698.

(11) Francisco, W. A.; Merkler, D. J.; Blackburn, N. J.; Klinman, J. P. Kinetic Mechanism and Intrinsic Isotope Effects for the Peptidylglycine α-Amidating Enzyme Reaction. *Biochemistry* **1998**, *37*, 8244-8252.

(12) Tian, G.; Berry, J. A.; Klinman, J. P. Oxygen-18 Kinetic Isotope Effects in the Dopamine β-Monooxygenase Reaction: Evidence for a New Chemical Mechanism in Non-Heme, Metallomonooxygenase. *Biochemistry* **1994**, *33*, 226-234.

(13) Miller, S. M.; Klinman, J. P. Magnitude of Intrinsic Isotope Effects in the Dopamine β-Monooxygenase Reaction. *Biochemistry* **1983**, *22*, 3091-3096.

(14) Hess, C. R.; McGuirl, M. M.; Klinman, J. P. Mechanism of the Insect Enzyme, Tyramine β-Monooxygenase, Reveals Differences from the Mammalian Enzyme, Dopamine β-Monooxygenase. *J. Biol. Chem.* **2008**, *283*, 3042-3049.

(15) Francisco, W. A.; Knapp, M. J.; Blackburn, N. J.; Klinman, J. P. Hydrogen Tunneling in Peptidylglycine α-Hydroxylating Monooxygenase. *J. Am. Chem. Soc.* **2002**, *124*, 8194-8195.

(16) Prigge, S. T.; Eipper, B. A.; Mains, R. E.; Amzel, L. M. Dioxygen Binds End-On to Mononuclear Copper in a Precatalytic Enzyme Complex. *Science* **2004**, *304*, 864-867.

(17) Cowley, R. E.; Tian, L.; Solomon, E. I. Mechanism of O_2 activation and substrate hydroxylation in noncoupled binuclear copper monooxygenases. *Proc. Natl. Acad. Sci. U.S.A.* **2016**, *113*, 12035-12040.

(18) Chen, P.; Solomon, E. I. Oxygen Activation by the Noncoupled Binuclear Copper Site in Peptidylglycine α-Hydroxylating Monooxygenase. Reaction Mechanism and Role of the Noncoupled Nature of the Active Site. *J. Am. Chem. Soc.* **2004**, *126*, 4991-5000.

(19) Elwell, C. E.; Gagnon, N. L.; Neisen, B. D.; Dhar, D.; Spaeth, A. D.; Yee, G. M.; Tolman, W. B. Copper-Oxygen Complexes Revisited: Structures, Spectroscopy, and Reactivity. *Chem. Rev.* **2017**, *117*, 2059-2107.

(20) Mirica, L. M.; Ottenwaelder, X.; Stack, T. D. P. Structure and Spectroscopy of Copper-Dioxygen Complexes. *Chem. Rev.* **2004**, *104*, 1013-1045.

(21) Karlin, K. D.; Wei, N.; Jung, B.; Kaderli, S.; Zuberbuehler, A. D. Kinetic, Thermodynamic, and Spectral Characterization of the Primary Cu-O_2 Adduct in a Reversibly Formed and Structurally Characterized Peroxo-Dicopper(II) Complex. *J. Am. Chem. Soc.* **1991**, *113*, 5868-5870.

(22) Karlin, K. D.; Kaderli, S.; Zuberbühler, A. D. Kinetics and Thermodynamics of Copper(I)/Dioxygen Interaction. *Acc. Chem. Res.* **1997**, *30*, 139-147.

(23) Bhadra, M.; Lee, J. Y. C.; Cowley, R. E.; Kim, S.; Siegler, M. A.; Solomon, E. I.; Karlin, K. D. Intramolecular Hydrogen Bonding Enhances Stability and Reactivity of Mononuclear Cupric Superoxide Complexes. *J. Am. Chem. Soc.* **2018**, *140*, 9042-9045.

(24) Fujisawa, K.; Tanaka, M.; Moro-oka, Y.; Kitajima, N., A Monomeric Side-On Superoxocopper(II) Complex: Cu(O_2)(HB(3-tBu-5-iPrpz)$_3$). *J. Am. Chem. Soc.* **1994**, *116*, 12079-12080.

(25) Aboelella, N. W.; Lewis, E. A.; Reynolds, A. M.; Brennessel, W. W.; Cramer, C. J.; Tolman, W. B. Snapshots of Dioxygen Activation by Copper: The Structure of a 1:1 Cu/O_2 Adduct and Its Use in Syntheses of Asymmetric Bis(μ-oxo) Complexes. *J. Am. Chem. Soc.* **2002**, *124*, 10660-10661.

(26) Reynolds, A. M.; Gherman, B. F.; Cramer, C. J.; Tolman, W. B. Characterization of a 1:1 Cu-O_2 Adduct Supported by an Anilido Imine Ligand. *Inorg. Chem.* **2005,** *44*, 6989-6997.

(27) Iovan, D. A.; Wrobel, A. T.; McClelland, A. A.; Scharf, A. B.; Edouard, G. A.; Betley, T. A. Reactivity of a stable copper–dioxygen complex. *Chem. Commun.* **2017**, *53*, 10306-10309.

(28) Aboelella, N. W.; Kryatov, S. V.; Gherman, B. F.; Brennessel, W. W.; Young, V. G., Jr.; Sarangi, R.; Rybak-Akimova, E. V.; Hodgson, K. O.; Hedman, B.; Solomon, E. I.; Cramer, C. J.; Tolman, W. B. Dioxygen Activation at a Single Copper Site: Structure, Bonding, and Mechanism of Formation of 1:1 Cu-O_2 Adducts. *J. Am. Chem. Soc.* **2004**, *126*, 16896-16911.

(29) Spencer, D. J. E.; Aboelella, N. W.; Reynolds, A. M.; Holland, P. L.; Tolman, W. B. β-Diketiminate Ligand Backbone Structural Effects on Cu(I)/O_2 Reactivity: Unique Copper-Superoxo and Bis(μ-oxo) Complexes. *J. Am. Chem. Soc.* **2002**, *124*, 2108-2109.

(30) Chen, P.; Root, D. E.; Campochiaro, C.; Fujisawa, K.; Solomon, E. I. Spectroscopic and Electronic Structure Studies of the Diamagnetic Side-On CuII-Superoxo Complex $Cu(O_2)$[HB(3-R-5-^{i}Prpz)$_3$]: Antiferromagnetic Coupling versus Covalent Delocalization. *J. Am. Chem. Soc.* **2003**, *125*, 466-474.

(31) Schatz, M.; Raab, V.; Foxon, S. P.; Brehm, G.; Schneider, S.; Reiher, M.; Holthausen, M. C.; Sundermeyer, J.; Schindler, S. Combined Spectroscopic and Theoretical Evidence for a Persistent End-On Copper Superoxo Complex. *Angew. Chem. Int. Ed.* **2004**, *43*, 4360-4363.

(32) Würtele, C.; Gaoutchenova, E.; Harms, K.; Holthausen, M. C.; Sundermeyer, J.; Schindler, S. Crystallographic Characterization of a Synthetic 1:1 End-On Copper Dioxygen Adduct Complex. *Angew. Chem. Int. Ed.* **2006**, *45*, 3867-3869.

(33) Lanci, M. P.; Smirnov, V. V.; Cramer, C. J.; Gauchenova, E. V.; Sundermeyer, J.; Roth, J. P. Isotopic Probing of Molecular Oxygen Activation at Copper(I) Sites. *J. Am. Chem. Soc.* **2007**, *129*, 14697-14709.

(34) Kobayashi, Y.; Ohkubo, K.; Nomura, T.; Kubo, M.; Fujieda, N.; Sugimoto, H.; Fukuzumi, S.; Goto, K.; Ogura, T.; Itoh, S. Copper(I)-Dioxygen Reactivity in a Sterically Demanding Tripodal Tetradentate tren Ligand: Formation and Reactivity of a Mononuclear Copper(II) End-On Superoxo Complex. *Eur. J. Inorg. Chem.* **2012**, 4574-4578.

(35) Donoghue, P. J.; Gupta, A. K.; Boyce, D. W.; Cramer, C. J.; Tolman, W. B. An Anionic, Tetragonal Copper(II) Superoxide Complex. *J. Am. Chem. Soc.* **2010**, *132*, 15869-15871.

(36) Maiti, D.; Lee, D.-H.; Gaoutchenova, K.; Würtele, C.; Holthausen, M. C.; Narducci Sarjeant, A. A.; Sundermeyer, J.; Schindler, S.; Karlin, K. D. Reactions of a Copper(II) Superoxo Complex Lead to C-H and O-H Substrate Oxygenation: Modeling Copper-Monooxygenase C-H Hydroxylation. *Angew. Chem. Int. Ed.* **2008**, *47*, 82-85.

(37) Bailey, W. D.; Dhar, D.; Cramblitt, A. C.; Tolman, W. B. Mechanistic Dichotomy in Proton-Coupled Electron-Transfer Reactions of Phenols with a Copper Superoxide Complex. *J. Am. Chem. Soc.* **2019**, *141*, 5470-5480.

(38) Bailey, W. D.; Gagnon, N. L.; Elwell, C. E.; Cramblitt, A. C.; Bouchey, C. J.; Tolman, W. B. Revisiting the Synthesis and Nucleophilic Reactivity of an Anionic Copper Superoxide Complex. *Inorg. Chem.* **2019**, *58*, 4706-4711.

(39) Pirovano, P.; Magherusan, A. M.; McGlynn, C.; Ure, A.; Lynes, A.; McDonald, A. R. Nucleophilic Reactivity of a Copper(II)-Superoxide Complex. *Angew. Chem. Int. Ed.* **2014**, *53*, 5946-5950.

(40) Itoh, S. Developing Mononuclear Copper-Active-Oxygen Complexes Relevant to Reactive Intermediates of Biological Oxidation Reactions. *Acc. Chem. Res.* **2015**, *48*, 2066-2074.

(41) Tano, T.; Okubo, Y.; Kunishita, A.; Kubo, M.; Sugimoto, H.; Fujieda, N.; Ogura, T.; Itoh, S. Redox Properties of a Mononuclear Copper(II)-Superoxide Complex. *Inorg. Chem.* **2013**, *52*, 10431-10437.

(42) Kunishita, A.; Kubo, M.; Sugimoto, H.; Ogura, T.; Sato, K.; Takui, T.; Itoh, S. Mononuclear Copper(II)-Superoxo Complexes that Mimic the Structure and Reactivity of the Active Centers of PHM and DβM. *J. Am. Chem. Soc.* **2009**, *131*, 2788-2789.

(43) Kunishita, A.; Ertem, M. Z.; Okubo, Y.; Tano, T.; Sugimoto, H.; Ohkubo, K.; Fujieda, N.; Fukuzumi, S.; Cramer, C. J.; Itoh, S. Active Site Models for the Cu_A Site of Peptidylglycine α-Hydroxylating Monooxygenase and Dopamine β-Monooxygenase. *Inorg. Chem.* **2012**, *51*, 9465-9480.

(44) Zhang, C. X.; Kaderli, S.; Costas, M.; Kim, E.-i.; Neuhold, Y.-M.; Karlin, K. D.; Zuberbühler, A. D. Copper(I)-Dioxygen Reactivity of $[(L)Cu^{I}]^{+}$ (L = Tris(2-pyridylmethyl)amine): Kinetic/ Thermodynamic and Spectroscopic Studies Concerning the Formation of Cu-O_2 and Cu_2-O_2 Adducts as a Function of Solvent Medium and 4-Pyridyl Ligand Substituent Variations. *Inorg. Chem.* **2003**, *42*, 1807-1824.

(45) Maiti, D.; Fry, H. C.; Woertink, J. S.; Vance, M. A.; Solomon, E. I.; Karlin, K. D. A 1:1 Copper-Dioxygen Adduct is an End-on Bound Superoxo Copper(II) Complex which Undergoes Oxygenation Reactions with Phenols. *J. Am. Chem. Soc.* **2007**, *129*, 264-265.

(46) Lee, J. Y.; Peterson, R. L.; Ohkubo, K.; Garcia-Bosch, I.; Himes, R. A.; Woertink, J.; Moore, C. D.; Solomon, E. I.; Fukuzumi, S.; Karlin, K. D. Mechanistic Insights into the Oxidation of Substituted Phenols via Hydrogen Atom Abstraction by a Cupric-Superoxo Complex. *J. Am. Chem. Soc.* **2014,** *136*, 9925-9937.

(47) Peterson, R. L.; Himes, R. A.; Kotani, H.; Suenobu, T.; Tian, L.; Siegler, M. A.; Solomon, E. I.; Fukuzumi, S.; Karlin, K. D. Cupric Superoxo-Mediated Intermolecular C-H Activation Chemistry. *J. Am. Chem. Soc.* **2011**, *133*, 1702-1705.

(48) Diaz, D. E.; Quist, D. A.; Herzog, A. E.; Schaefer, A. W.; Kipouros, I.; Bhadra, M.; Solomon, E. I.; Karlin, K. D. Impact of Intramolecular Hydrogen Bonding on the Reactivity of Cupric Superoxide Complexes with O–H and C–H Substrates. *Angew. Chem. Int. Ed.* **2019**, *58*, 17572-17576.

(49) Addison, A. W.; Rao, T. N.; Reedijk, J.; van Rijn, J.; Verschoor, G. C. Synthesis, structure, and spectroscopic properties of copper(II) compounds containing nitrogen–sulphur donor ligands; the crystal and molecular structure of aqua[1,7-bis(*N*-methylbenzimidazol-2′-yl)-2,6-dithiaheptane]copper(II) perchlorate. *Dalton Trans.* **1984**, 1349-1356.

(50) Kunishita, A.; Kubo, M.; Ishimaru, H.; Ogura, T.; Sugimoto, H.; Itoh, S. H_2O_2-Reactivity of Copper(II) Complexes Supported by Tris[(pyridin-2-yl)methyl]amine Ligands with 6-Phenyl Substituents. *Inorg. Chem.* **2008,** *47*, 12032-12039.

(51) Chuang, C.-l.; Lim, K.; Chen, Q.; Zubieta, J.; Canary, J. W. Synthesis, Cyclic Voltammetry, and x-ray Crystal Structures of Copper(I) and Copper(II) Complexes of Tris((6-phenyl-2-pyridyl)methyl)amine (TPPA). *Inorg. Chem.* **1995**, *34*, 2562-2568.

(52) Bordwell, F. G.; Zhang, X.-M. Acidities and homolytic bond dissociation enthalpies of 4-substituted-2,6-di-tert-butylphenols. *J. Phys. Org. Chem.* **1995**, *8*, 529-535.

(53) Wu, T.; MacMillan, S. N.; Rajabimoghadam, K.; Siegler, M. A.; Lancaster, K. M.; Garcia-Bosch, I. Structure, Spectroscopy, and Reactivity of a Mononuclear Copper Hydroxide Complex in Three Molecular Oxidation States. *J. Am. Chem. Soc.* **2020,** *142*, 12265-12276.

(54) Kim, S.; Saracini, C.; Siegler, M. A.; Drichko, N.; Karlin, K. D. Coordination Chemistry and Reactivity of a Cupric Hydroperoxide Species Featuring a Proximal H-Bonding Substituent. *Inorg. Chem.* **2012**, *51*, 12603-12605.

(55) Choi, Y. J.; Cho, K.-B.; Kubo, M.; Ogura, T.; Karlin, K. D.; Cho, J.; Nam, W. Spectroscopic and computational characterization of Cu^{II}-OOR (R = H or cumyl) complexes bearing a Me_6-tren ligand. *Dalton Trans.* **2011**, *40*, 2234-2241.

(56) Yamaguchi, S.; Nagatomo, S.; Kitagawa, T.; Funahashi, Y.; Ozawa, T.; Jitsukawa, K.; Masuda, H. Copper Hydroperoxo Species Activated by Hydrogen-Bonding Interaction with Its Distal Oxygen. *Inorg. Chem.* **2003**, *42*, 6968-6970.

(57) Wada, A.; Harata, M.; Hasegawa, K.; Jitsukawa, K.; Masuda, H.; Mukai, M.; Kitagawa, T.; Einaga, H. Structural and Spectroscopic Characterization of a Mononuclear Hydroperoxo–Copper(II) Complex with Tripodal Pyridylamine Ligands. *Angew. Chem. Int. Ed.* **1998**, *37*, 798-799.

(58) Kunishita, A.; Scanlon, J. D.; Ishimaru, H.; Honda, K.; Ogura, T.; Suzuki, M.; Cramer, C. J.; Itoh, S. Reactions of Copper(II)-H_2O_2 Adducts Supported by Tridentate Bis(2-pyridylmethyl)amine Ligands: Sensitivity to Solvent and Variations in Ligand Substitution. *Inorg. Chem.* **2008**, *47*, 8222-8232.

(59) Warren, J. J.; Tronic, T. A.; Mayer, J. M. Thermochemistry of Proton-Coupled Electron Transfer Reagents and its Implications. *Chem. Rev.* **2010**, *110*, 6961-7001.

(60) Zhu, X.-Q.; Zhang, M.-T.; Yu, A.; Wang, C.-H.; Cheng, J.-P. Hydride, Hydrogen Atom, Proton, and Electron Transfer Driving Forces of Various Five-Membered Heterocyclic Organic Hydrides and Their Reaction Intermediates in Acetonitrile. *J. Am. Chem. Soc.* **2008**, *130*, 2501-2516.

(61) Osako, T.; Ohkubo, K.; Taki, M.; Tachi, Y.; Fukuzumi, S.; Itoh, S. Oxidation Mechanism of Phenols by Dicopper−Dioxygen (Cu_2/O_2) Complexes. *J. Am. Chem. Soc.* **2003**, *125*, 11027-11033.

(62) Fukuzumi, S.; Shimoosako, K.; Suenobu, T.; Watanabe, Y. Mechanisms of Hydrogen-, Oxygen-, and Electron-Transfer Reactions of Cumylperoxyl Radical. *J. Am. Chem. Soc.* **2003**, *125*, 9074-9082.

(63) Ram, M. S.; Hupp, J. T. Linear Free Energy Relations for Multielectron Transfer Kinetics: A Brief Look at the Brønsted/Tafel Analogy. *J. Phys. Chem.* **1990**, *94*, 2378-2380.

(64) Weatherly, S. C.; Yang, I. V.; Thorp, H. H. Proton-Coupled Electron Transfer in Duplex DNA: Driving Force Dependence and Isotope Effects on Electrocatalytic Oxidation of Guanine. *J. Am. Chem. Soc.* **2001**, *123*, 1236-1237.

(65) Guttenplan, J. B.; Cohen, S. G. Triplet Energies, Reduction Potentials, and Ionization Potentials in Carbonyl-Donor Partial Charge-Transfer Interactions. I. *J. Am. Chem. Soc.* **1972**, *94*, 4040-4042.

(66) Wagner, P. J.; Lam, H. M. H. Charge-Transfer Quenching of Triplet α-Trifluoroacetophenones. *J. Am. Chem. Soc.* **1980**, *102*, 4167-4172.

(67) Connelly, N. G.; Geiger, W. E. Chemical Redox Agents for Organometallic Chemistry. *Chem. Rev.* **1996**, *96*, 877-910.

(68) Kochi, J. K. *Free radicals. Edited by Jay K. Kochi*. Wiley: New York, 1973.

(69) Halliwell, B.; Gutteridge, J. M. C. *Free Radicals in Biology and Medicine*. 5 ed.; Oxford University Press: Oxford, 2015; p 944.

(70) Mayer, J. M. Understanding Hydrogen Atom Transfer: From Bond Strengths to Marcus Theory. *Acc. Chem. Res.* **2011**, *44*, 36-46.

(71) Roth, J. P.; Yoder, J. C.; Won, T. J.; Mayer, J. M. Application of the Marcus Cross Relation to Hydrogen Atom Transfer Reactions. *Science* **2001**, *294*, 2524-2526.

(72) Warren, J. J.; Mayer, J. M. Predicting organic hydrogen atom transfer rate constants using the Marcus cross relation. *Proc. Natl. Acad. Sci. U.S.A.* **2010**, *107*, 5282-5287.

(73) Sutin, N. Theory of Electron Transfer Reactions: Insights and Hindsights. *Prog. Inorg. Chem.* **1983**, *30*, 441-498.

(74) Mayer, J. M Proton-Coupled Electron Transfer: A Reaction Chemist's View. *Annu. Rev. Phys. Chem.* **2004**, *55*, 363-390.

(75) Kindermann, N.; Günes, C.-J.; Dechert, S.; Meyer, F. Hydrogen Atom Abstraction Thermodynamics of a μ-1,2-Superoxo Dicopper(II) Complex. *J. Am. Chem. Soc.* **2017**, *139*, 9831-9834.

(76) Sacramento, J. J. D.; Goldberg, D. P. The hydrogen atom transfer reactivity of a porphyrinoid cobalt superoxide complex. *Chem. Commun.* **2019**, *55*, 913-916.

(77) Dhar, D.; Yee, G. M.; Spaeth, A. D.; Boyce, D. W.; Zhang, H.; Dereli, B.; Cramer, C. J.; Tolman, W. B. Perturbing the Copper(III)-Hydroxide Unit through Ligand Structural Variation. *J. Am. Chem. Soc.* **2016**, *138*, 356-368.

(78) Donoghue, P. J.; Tehranchi, J.; Cramer, C. J.; Sarangi, R.; Solomon, E. I.; Tolman, W. B. Rapid C-H Bond Activation by a Monocopper(III)-Hydroxide Complex. *J. Am. Chem. Soc.* **2011**, *133*, 17602-17605.

(79) Devi, T.; Lee, Y.-M.; Jung, J.; Sankaralingam, M.; Nam, W.; Fukuzumi, S. A Chromium(III)-Superoxo Complex as a Three-Electron Oxidant with a Large Tunneling Effect in Multi-Electron Oxidation of NADH Analogues. *Angew. Chem. Int. Ed.* **2017**, *56*, 3510-3515.

(80) Knapp, M. J.; Rickert, K.; Klinman, J. P. Temperature-Dependent Isotope Effects in Soybean Lipoxygenase-1: Correlating Hydrogen Tunneling with Protein Dynamics. *J. Am. Chem. Soc.* **2002**, *124*, 3865-3874.

(81) Klinman, J. P.; Offenbacher, A. R. Understanding Biological Hydrogen Transfer Through the Lens of Temperature Dependent Kinetic Isotope Effects. *Acc. Chem. Res.* **2018**, *51*, 1966-1974.

(82) Kohen, A.; Klinman, J. P. Enzyme Catalysis: Beyond Classical Paradigms. *Acc. Chem. Res.* **1998**, *31*, 397-404.

(83) Kwart, H. Temperature Dependence of the Primary Kinetic Hydrogen Isotope Effect as a Mechanistic Criterion. *Acc. Chem. Res.* **1982**, *15*, 401-408.

(84) Cho, J.; Woo, J.; Nam, W. An "End-On" Chromium(III)-Superoxo Complex: Crystallographic and Spectroscopic Characterization and Reactivity in C−H Bond Activation of Hydrocarbons. *J. Am. Chem. Soc.* **2010**, *132*, 5958-5959.

(85) Bhadra, M.; Transue, W. J.; Lim, H.; Cowley, R. E.; Lee, J. Y. C.; Siegler, M. A.; Josephs, P.; Henkel, G.; Lerch, M.; Schindler, S.; Neuba, A.; Hodgson, K. O.; Hedman, B.; Solomon, E. I.; Karlin, K. D. A Thioether-Ligated Cupric Superoxide Model with Hydrogen Atom Abstraction Reactivity. *J. Am. Chem. Soc.* **2021**, *143*, 3707-3713.